Cell Reports

Article

Protein quality and quantity influence the effect of dietary fat on weight gain and tissue partitioning via host-microbiota changes

Graphical abstract

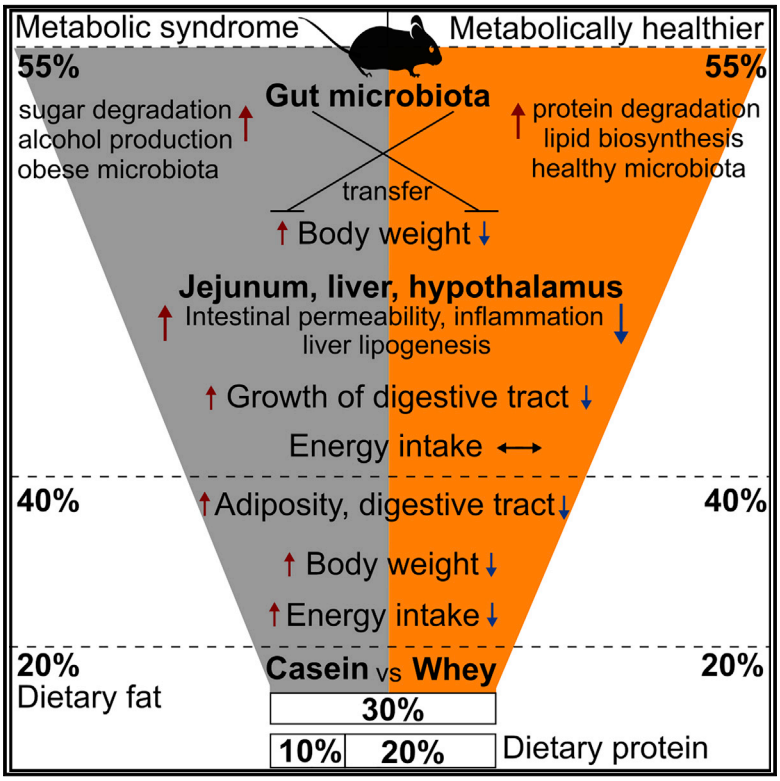

Highlights

- High dietary fat interacts with high casein and causes tissue expansion in mice
- Changing the protein from casein to whey blunts tissue accruement
- Alterations in gut microbiota are related to protein quality
- Casein microbiota increases body size, and whey microbiota has the opposite effect

Authors

Oleksandr Nychyk, Wiley Barton, Agata M. Rudolf, ..., Paul D. Cotter, John R. Speakman, Kanishka N. Nilaweera

Correspondence

kanishka.nilaweera@teagasc.ie

In brief

High dietary fat intake causes excessive weight gain. Nychyk et al. show that, in mice, the detrimental effects of dietary fat are worse when it is consumed in high quantities and with milk-associated casein protein, whereas its effects are reduced dramatically when co-ingested with whey, an alternative milk-associated protein.

Nychyk et al., 2021, Cell Reports *35*, 109093
May 11, 2021 © 2021 The Authors.
https://doi.org/10.1016/j.celrep.2021.109093

CellPress

Cell Reports

CellPress
OPEN ACCESS

Article

Protein quality and quantity influence the effect of dietary fat on weight gain and tissue partitioning via host-microbiota changes

Oleksandr Nychyk,[1] Wiley Barton,[1,2] Agata M. Rudolf,[3] Serena Boscaini,[1,4] Aaron Walsh,[1] Thomaz F.S. Bastiaanssen,[4,5] Linda Giblin,[1,2] Paul Cormican,[6] Liang Chen,[7] Yolanda Piotrowicz,[8] Davina Derous,[8] Áine Fanning,[5] Xiaofei Yin,[9] Jim Grant,[10] Silvia Melgar,[5] Lorraine Brennan,[2,9] Sharon E. Mitchell,[8] John F. Cryan,[4,5] Jun Wang,[7] Paul D. Cotter,[1,2,5] John R. Speakman,[3,8,11,12] and Kanishka N. Nilaweera[1,2,13,*]

[1]Food Biosciences Department, Teagasc Food Research Centre, Moorepark, Fermoy, County Cork P61 C996, Ireland
[2]VistaMilk Research Centre, Teagasc, Moorepark, Fermoy, County Cork P61 C996, Ireland
[3]Key State Laboratory for Molecular Developmental Biology, Chinese Academy of Sciences, Beijing 100101, China
[4]Department of Anatomy and Neuroscience, University College Cork, Cork T12 YT20, Ireland
[5]APC Microbiome Ireland, University College Cork, Cork T12 YT20, Ireland
[6]Animal and Grassland Research and Innovation Centre, Teagasc, Grange, Dunsany, County Meath, Ireland
[7]CAS Key Laboratory for Pathogenic Microbiology and Immunology, Institute of Microbiology, Chinese Academy of Sciences, Beijing 100101, China
[8]School of Biological Sciences, University of Aberdeen, Aberdeen AB24 2TZ, UK
[9]School of Agriculture and Food Science, Institute of Food and Health and Conway Institute, University College Dublin, Dublin, Ireland
[10]Teagasc Food Research Centre, Ashtown, Dublin 15, Ireland
[11]CAS Center of Excellence in Animal Evolution and Genetics, Kunming Institute of Zoology, Kunming, China
[12]Center for Energy Metabolism and Reproduction, Shenzhen Institutes of Advanced Technology, Chinese Academy of Sciences, Shenzhen, Guangdong, China
[13]Lead contact
*Correspondence: kanishka.nilaweera@teagasc.ie
https://doi.org/10.1016/j.celrep.2021.109093

SUMMARY

We investigated how protein quantity (10%–30%) and quality (casein and whey) interact with dietary fat (20%–55%) to affect metabolic health in adult mice. Although dietary fat was the main driver of body weight gain and individual tissue weight, high (30%) casein intake accentuated and high whey intake reduced the negative metabolic aspects of high fat. Jejunum and liver transcriptomics revealed increased intestinal permeability, low-grade inflammation, altered lipid metabolism, and liver dysfunction in casein-fed but not whey-fed animals. These differential effects were accompanied by altered gut size and microbial functions related to amino acid degradation and lipid metabolism. Fecal microbiota transfer confirmed that the casein microbiota increases and the whey microbiota impedes weight gain. These data show that the effects of dietary fat on weight gain and tissue partitioning are further influenced by the quantity and quality of the associated protein, primarily via effects on the microbiota.

INTRODUCTION

The role of diet in driving body composition has been studied for many decades (Abete et al., 2010; McAllan et al., 2015), but little progress has been made toward understanding the molecular mechanisms involved. This is largely because most human and many animal studies use a rather simplified view of the interaction between diet and body composition, which we know to be heterogeneous constructs, with many adipose and lean tissue-associated subcompartments responding differently to energy challenges (Archer et al., 2018). Second, understanding the effects of diet have largely been based on simple manipulation of single macronutrients (Hu et al., 2018; Solon-Biet et al., 2014), whereas humans and animals rarely consume dietary macronutrients in isolation but in combination, which sometimes falls outside of the acceptable macronutrient distribution range (AMDR) of 20%–35% fat, 10%–35% protein, and 45%–65% carbohydrate (CHO) (Berryman et al., 2018; Wolfe et al., 2017). The interplay between dietary macronutrients and different tissues is understudied.

Of the macronutrients, dietary fat has historically attracted the most attention because its intake has increased in the last century, in line with the obesity epidemic (Caballero, 2007), driving energy intake (EI) and adiposity (Hu et al., 2018), in part because of microbial imbalance in the gut (Brun et al., 2007; Mao et al., 2013), leading to lipotoxicity, inflammation, and impaired glucose tolerance (Flegal et al., 2013; Hu et al., 2020). In contrast to dietary fat, intake of complex CHO and dietary fiber has declined during

This is an open access article under the CC BY-NC-ND license (http://creativecommons.org/licenses/by-nc-nd/4.0/).

the same period of the last century, whereas intake of dietary protein remained almost stable (Gortner, 1975; Hamilton and Anderson, 1992). Studies suggest that the proportion of total CHO in the diet (notably, high sugar intake and dietary fiber) differentially affects EI and weight gain (Ludwig et al., 2018; van Dam and Seidell, 2007). However, not all of these findings were confirmed by others (Hu et al., 2018; Smith et al., 2017). Additionally, much controversy exists regarding the effects of protein quantity and quality on body composition (Hu et al., 2018; Patel, 2015; Simpson and Raubenheimer, 2005) because different outcomes occur during the active growth stage (early life) versus adulthood. Although high protein intake during early childhood is associated with increased weight gain and adiposity, in part because of overstimulation of the growth hormone (GH)/insulin growth factor 1 (IGF-1) system (Hoppe et al., 2009; Pimpin et al., 2018), in adults, high-protein (30%) diets increase satiety, enhance energy expenditure, and improve metabolic health (Paddon-Jones et al., 2008), with further effects modulated by protein type (Hall et al., 2003), which, together, reduce fat mass and increase lean tissue mass. The differences in the activity of proteins are dependent, at least in part, on the associated amino acid quantity and composition. For example, the known improvement in the body composition associated with milk-derived whey proteins (Tahavorgar et al., 2014) appears to be due to the much higher essential amino acid composition compared with the corresponding milk-associated casein and plant and egg proteins (Gorissen et al., 2018). Beyond the dietary source, the gut microbiota also has the potential to alter the host nutrient supply. For instance, the microbial metabolism of dietary amino acids causes production of short-chain and branched-chain fatty acids that can significantly affect the health of the host (Lin et al., 2017; Neis et al., 2015).

Given the uncertainty regarding how different dietary macronutrient combinations affect the complex responses of all body tissues, here we wanted to find out to what extent 24 different body tissues were affected by the interaction between dietary fat and protein quantity and the source over and beyond the AMDR range. To test the effects of the proteins, we used casein and whey protein isolate (WPI), which differ substantially in their amino acid quantity and composition (Gorissen et al., 2018). We reasoned that there would be an interplay between dietary protein quality and quantity in the gut with the microbiome component, which would result in a changed host nutrient supply, and that this, in turn, would affect weight gain and tissue partitioning. Using adult male mice aged 20 weeks that were beyond the active growth phase, we show that a much more complex dietary interplay between protein type and quantity with dietary fat is required to change the microbiota and tissue responses (Figure 1A; study 1). This work formed the basis of a follow-up study that assessed the specific role of the microbiota in mediating the protein effects (Figure 1A; study 2).

RESULTS

Study 1, part 1: High (30%) whey protein content transiently reduced high dietary fat/low CHO (HFLC)-induced energy intake

20-week-old C57/BL6J mice were exposed for 12 weeks to a series of dietary treatments consisting of three different levels of dietary fat (20%, 40%, and 55% by energy) combined with three different levels of protein (10%, 20%, and 30% by energy) with casein (CAS) or WPI (18 diets in total with 11–12 animals per diet) (Figure 1A; Table S1; D17052701–D17052718). The CHO amount was reduced in parallel with an increase in dietary protein and fat. Univariate factorial ANOVA was used to analyze the effects of all three dietary factors on EI and body weight (BW). Only dietary fat content had a significant effect on average EI ($p = 1.51 \times 10^{-17}$) (Figure 1B; Table S2), where the average EIs of the entire study period and the first 6 weeks of the mice fed with 40% and 55% fat diets were higher than that of mice fed diets with 20% fat over the entire treatment period (Figure 1B). However, a transient effect of protein type and content was evident, where the average EI of the 30% WPI group was significantly lower than the average EI of the group with 30% CAS at 40% fat (Table S2; $p = 0.041$) over the first 6 weeks of diet exposure, which then normalized so that the overall effect showed a trend toward significance by the end of the treatment period ($p = 0.06$) (Figure 1B).

High whey protein chronically reduced HFLC-induced weight gain

The baseline BW was not significantly different between groups (one-way ANOVA F-statistic$_{(17, 192)} = 0.337$, $p = 0.994$) (Figure 1C). The BW varied significantly over 12 weeks of dietary treatment ($p < 0.0001$) (Figure 1C), with significant fat content, protein type, and content by time interaction ($F_{(44, 698)} = 2.9$, $p < 0.001$). In general, the increase in EI in the 40% and 55% fat groups was mirrored by an increase in BW (Figures 1C and S1A) over the treatment period (Figure 1D), with the most significant differences between 20% and 40% fat and 20% and 55% fat within each protein type (Figure S1A; Table S2). However, the final BW and BW gain were dependent on fat content, protein type, and protein content ($p = 0.031$ for BW, $p = 0.0022$ for BW gain). Animals on 30% CAS with 40% and 55% fat had significantly increased BW from week 2 onward relative to 20% fat ($p < 0.05$). In contrast, BWs of animals from 30% WPI groups were significantly lower than those of animals from 30% CAS groups from week 6 in the 40% fat group and from week 2 in the 55% fat group until week 12 ($p < 0.05$) (Figures 1C and S1A). This was reflected in BW gain; a strong effect on BW gain (84% reduction) was observed in WPI relative to CAS at 40% fat, and a mild effect (20% reduction) was present at 55% fat (Figure 1D). The stronger effect is likely to be due to the abovementioned transient (first 6-week period) reduction in EI in 30% WPI and 40% fat co-fed mice combined with an additional effect (related to microbiota; see below) that maintained the reduction in BW gain beyond the 6-week period (until the end of the study) (Figures 1C and 1D). The latter effect is again evident in 55% fat-fed mice with 30% WPI because these mice consumed the same amount of energy as 30% CAS-fed mice (Figure 1B) but continued to gain less weight (Figures 1C and 1D). This indicated a mismatch between energy supply to the host and its use/deposition at the end of the treatment period.

High WPI maintained the correlation between BW gain and tissue weight with HFLC feeding

Using a protocol published previously (Mitchell et al., 2015), a Z score-like transformation was applied to the 24 different tissues in study 1 using the median instead of the mean weights, and

A **Summary of experiments performed and main findings**

Study	Design	Main findings
1: Part 1: Manipulation of dietary fat (F)/protein (P) levels and protein quality (WPI, CAS)	· Adult C57BL/6 mice fed 20, 40 and 55% F combined with 10, 20 and 30% P each replicated with either casein (CAS) or whey protein isolate (WPI). · Main outcomes: energy intake (EI), body weight (BW) and adiposity.	· EI, BW and adiposity increased with dietary F. · Effect on BW gain was reduced by 30% WPI relative to 30% CAS (high) at both 40 and 55% F. · BW positively correlated with IGF-1 levels in high WPI at 40/55% F and this correlation was lost in corresponding CAS groups. · 30% WPI transiently reduced EI relative to CAS and only at 40% F.
1: Part 2: 30% WPI and CAS with 20-55% F.	· Measurement of tissue weight, serum hormones and metabolites. · Transcriptomic responses of the jejunum, liver and the hypothalamus. · Microbiome and metabolome-response of caecal contents.	· 30% WPI reduced adipose tissues (40% F) and the digestive tract (40 & 55% F), which were accompanied by reduced serum leptin, IGF-1, glucose and inflammatory markers. · Increased intestinal permeability, low-grade inflammation, altered lipid metabolism and liver dysfunction was associated with CAS, but not with WPI intake. · Increased amino acid and lipid metabolism in the bacteria was associated with growth of lean microbiota in WPI. · Faecal energy loss increased with WPI.
2: 30% WPI and CAS with 55% F	· Adult C57BL/6 mice fed the 2 diets for 4 weeks, followed by antibiotic treatment (4 weeks) and then transfer of WPI- or CAS-derived microbiome (4 weeks).	· WPI microbiota impeded BW gain in CAS-fed mice and the effect was overridden by CAS diet. · CAS microbiota promoted BW gain in WPI-fed mice.

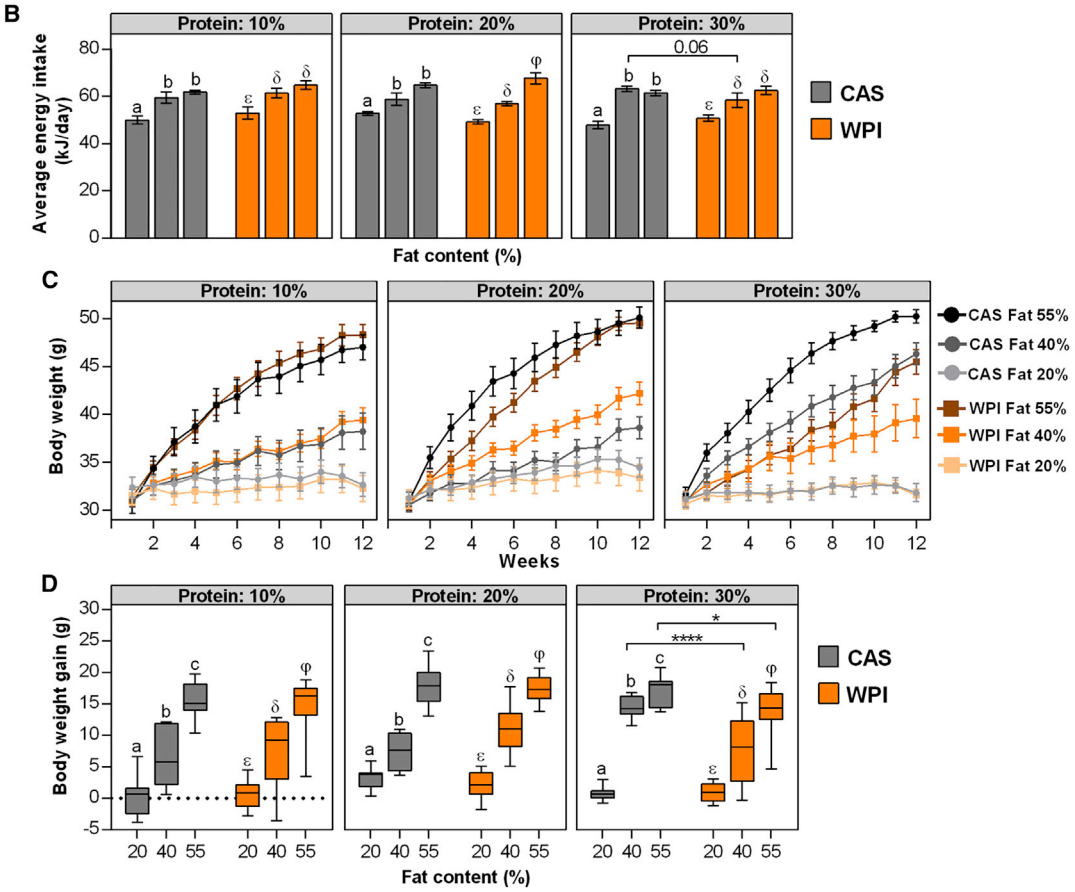

Figure 1. Effect of macronutrients on energy intake and body weight

Summary of experiments performed and main findings (A), average daily EI per animal over 12 weeks (B), weekly body weight (BW; grams; C), and BW gain after 12 weeks of treatment (D). Groups were compared by fat content (CAS, English; WPI, Greek letters) and protein type (CAS versus WPI, *$p < 0.05$, **$p < 0.01$, ***$p < 0.001$, ****$p < 0.0001$; B–D). Values are represented as mean ± SEM (B and D) and as boxplots (C). n = 4 (cages in B) and 11–12 (animals in C and D) biologically independent samples. Groups with the same letters are not significantly different ($p > 0.05$). See Table S2 for the results of pairwise comparison of EI and BW gain according to protein content.

then principal-component analysis (PCA) was used to investigate the correlation patterns between different tissues with variable fat content, protein type, and content. The clustering analysis revealed that fat and protein content explained part of the variance observed in the PCA (PERMANOVA [permutational multivariate analysis of variance], $p < 0.001$ for both), whereas protein type

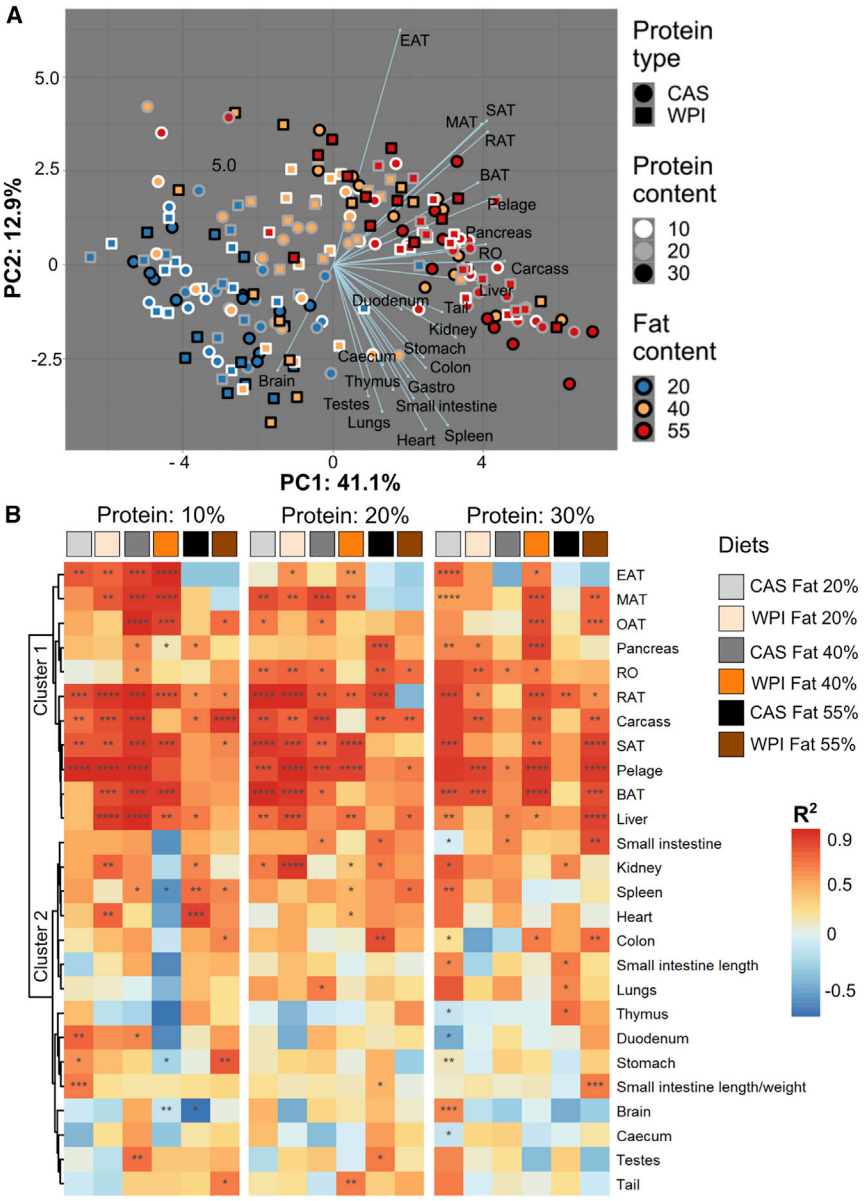

Figure 2. PCA correlation biplot of recorded tissue weights and correlation matrix showing the magnitude of correlation between BW and tissue weights of animals after dietary interventions

(A) PCA clustering analysis of body composition based on recorded weights of 24 different tissues. The loadings (tissues) magnitude is 100×. Median-based *Z* score metrics was used to perform a clustering analysis. The lines represent the direction of the tissue weights toward macronutrients. See Table S2 for the results of pairwise comparison of body composition between different diets.

(B) Correlation coefficients and p values of BW versus tissue weight. The scale for the correlations: increasing intensity of brown indicates positive correlation, and increasing intensity of blue indicates negative correlation. The dendrogram shows the similarity in responses of the different organs to BW changes. EAT, epidydimal AT; MAT, mesenteric AT; SAT, subcutaneous AT; RAT, retroperitoneal AT; BAT, brown AT; OAT, omental AT; AT, adipose tissue; RO, reproductive accessory organs. p value range: *p < 0.05, **p < 0.01, ***p < 0.001, ****p < 0.0001). n = 11–12 biologically independent samples. See Figure S1B for correlation between IGF-1 and tissue weight.

had a minor effect (PERMANOVA, p = 0.056). The most visible clustering was based on dietary fat content separating 20% from 55% fat (Figure 2A). The results of a pairwise comparison between diets further confirm that dietary fat was the main source of variation in tissue weight (body composition) (Table S2). Interestingly, the effect of protein type on tissue weight was only evident in animals on HFLC (40%, 55%) with high protein content (30%). A cluster analysis illustrated that the body composition is regulated by all three dietary factors only in HFLC and high protein content diets. The biplot shows that sizes of adipose tissue (AT) depots, liver, pelage, carcass, pancreas, and reproductive organs were strongly associated with high-fat diets (HFDs). In fact, investigation of the correlation between BW and organ weight revealed that these organs (except the pancreas) belong to the same cluster (cluster 1) (Figure 2B). The BW/tissue weight correlation showed that the digestive system and the two vital organs (heart and spleen) cluster together (cluster 2) with the reproductive organs and the tail (Figure 2B). On 10% and 20% protein diets with 20% and 40% fat, cluster 1-related tissues (AT depots, liver, pelage, and carcass) are strongly and positively correlated with BW, but this correlation pattern was lost for most of these tissues at higher fat content (55%) and even when 30% CAS was used (Figure 2B). However, changing the protein type to WPI (30%) retained the correlation at 40% and 55% fat. In particular, the AT depots and the liver were positively correlated with BW in 30% WPI groups at 40% and 55% fat, and this correlation was absent in the corresponding 30% CAS groups. This correlation extended to IGF-1 levels despite some changes in hierarchical clustering (Figure S1B).

In summary, intake of 30% WPI reduced the BW gain and allowed mice to maintain the correlation between BW/IGF-1 and tissue weight during high-fat feeding (40% and 55% fat). Therefore, in the subsequent experiments, we focused on delineating the effects of fixed 30% (high) protein intake with variable fat content and protein type.

Study 1, part 2: Effects of high WPI are evident in tissue weight and hormone levels

On 40% and 55% fat diets, intake of 30% WPI reduced the weight of individual components of the gastrointestinal tract (including

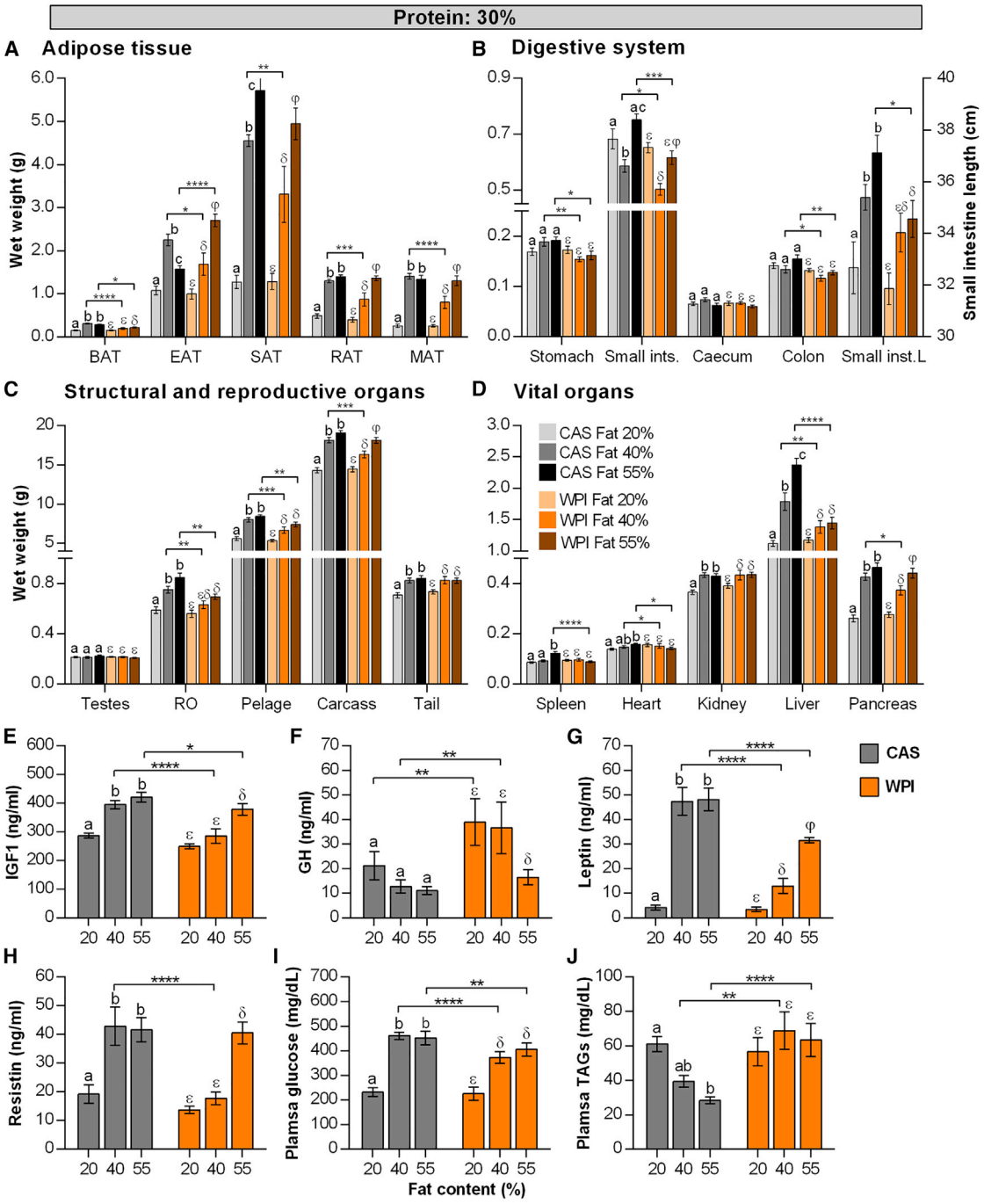

Figure 3. Effect of 30% protein with variable protein types and fat content on wet tissue weights, small intestine length, and circulating factors

Effect of 30% protein with variable protein type and fat content (percent energy) on (A–D) wet tissue weights (grams), small intestine length (centimeters, B), and circulating factors (E–J). Values are represented as mean ± SEM. Groups were compared within different fat contents (CAS, English; WPI, Greek letters) and protein types (CAS versus WPI, *p < 0.05, **p < 0.01, ***p < 0.001, ****p < 0.0001). n = 11–12 (A–D) and 9–12 (E–J) biologically independent samples; n = 2 technical replicates (E–J).

intestinal length), structural and reproductive accessory organs, and several vital organs relative to the equivalent CAS-fed groups (Figures 3B–3D). However, the effect of WPI on AT differed between 40% and 55% fat. On 40% fat diets, WPI significantly reduced the weight of individual fat depots relative to CAS, and this effect was not present on 55% fat diets, with the exception of brown AT (Figure 3A) and omental AT (CAS = 122 ± 7 mg, WPI = 73 ± 9 mg, p < 0.05). The opposite response was observed

for epididymal AT (EAT) at 55% fat, the WPI group showed a significant increase in EAT weight relative to CAS. The EAT weight increased in parallel with upregulation of genes involved in lipogenesis and glucose uptake (*Fasn* and *Glut4*), and this effect was not observed in subcutaneous AT (SAT; Figures S6F and S6G). In addition, the small intestine weight-to-length ratio was reduced significantly in WPI relative to CAS at 55% fat (CAS = 20.2 ± 0.4 mg/cm, WPI = 17.7 ± 0.5 mg/cm, $p < 0.05$), suggesting that the WPI group would have had a lower cell number and/or nutrient load per centimeter of tissue than the CAS group. In line with previous studies (Kakimoto and Kowaltowski, 2016), the liver weight more than doubled (111% increase) between 20% and 55% fat in CAS-fed animals and only increased by 23% in the corresponding WPI-fed animals (Figure 3D), suggesting ectopic fat accumulation in the livers of CAS- but not WPI-fed mouse groups. High-fat feeding could also induce splenomegaly, leading to accumulation of macrophages and other cellular/histological changes in the spleen (Altunkaynak et al., 2007; Buchan et al., 2018). Importantly, intake of 40% and 55% fat induced splenomegaly in those eating CAS, whereas the increase of dietary fat in the corresponding WPI diets did not change the weight of the spleen (Figure 3D).

Consistent with the tissue responses, IGF-1, leptin, resistin, and glucose increased in 30% CAS with the 40% and 55% fat groups relative to the 20% fat group, and an opposite response was observed for triglycerides (TAGs) (Figures 3E and 3G–3J), alongside an increase in AT weight (Figure 3A). The well-established IGF-1/GH coupling was not apparent; despite a rise in IGF-1 in plasma, GH did not respond to the increasing fat in CAS diets (Figure 3F).

On 30% WPI diets, and in contrast to CAS, IGF-1, resistin, and GH remained unchanged between 20% and 40% fat, with a modest increase in plasma leptin and glucose; however, a further increase in dietary fat led to increased IGF-1, resistin, and leptin and, consistent with IGF-1/GH coupling, decreased GH levels in the plasma (Figures 3E–3I). Overall, most metabolic parameters were improved by intake of 30% WPI compared with CAS with HFLC, with the exception of TAG levels, which did not change within the 30% WPI groups and was elevated in the plasma in 40% and 55% fat groups compared with the respective CAS groups (Figure 3J). This highlights a dissociation of TAG storage and tissue expansion in the WPI groups. High fat intake increased plasma cytokine levels (tumor necrosis factor α [TNF-α], monocyte chemoattractant protein-1 [CCL2/MCP-1], interleukin-15 [IL-15], and IP-10) in CAS but not in WPI groups, with an exception of a small increase in IL-15 in WPI from 40% to 55% fat (Figures S2A–S2D).

High WPI protects the jejunum from high-fat-induced inflammation and maintains intestinal barrier integrity

Transcriptome analysis (Table S3) revealed that WPI increased expression of the anti-inflammatory epoxygenase P450 gene family (Figure 4A) and reduced expression of the *Pla2g4c* gene, involved in production of eicosanoid progenitors from arachidonic acid, along with eicosanoid signaling in WPI relative to CAS in 55% fat (Figures 4A and 4C). In line with an effect on *Pla2g4c*, where this gene and *Clca3b* are associated with Paneth cell hyperplasia and increased mucus production, *Muc4* and *Muc13* mRNA were reduced in WPI relative to CAS (Figure 4A). Remodeling of the epithelium was evident as expression of adherent junction proteins (except Jam2) increased in WPI in 40% and 55% fat relative to the 20% fat group (Figure 4A), and the intestinal epithelial barrier function-related protein tyrosine phosphatase 22 (*Ptpn22*) increased in WPI relative to CAS in 40% and 55% fat (Figure 4B). This was accompanied by a reduction in lipopolysaccharide (LPS)-induced TLR4-CD14 activation in immune cells, specifically in 55% fat (Figures 4C and S2F).

Upstream regulators (lipid A and CD14), known to enhance intestinal permeability, were inhibited, and a reduced transcriptomic profile was seen for mast cells (CD2), cytotoxic CD8 T cells, T helper cytokines (Th1 and Th17), and their associated upstream regulators (interferon gamma [IFNG]and ILs) and canonical pathways (inducible T cell co-stimulator [iCOS] and nuclear factor κB [NF-κβ] signaling) in WPI compared with CAS in 55% fat groups (Figures 4C, causal networks, and S2E; Table S4). These results were reflected (and to some extent in the 40% fat group) by expression of genes encoding pro-inflammatory ligands, their receptors (ILs and chemokines) and regulators (IL-10RA), genes involved in immune cell migration (*Ccr6*, *Itgb7*, etc.) and activation (Toll-like receptors [TLRs] and downstream MYD88), and stimulation of an inflammatory response in the gut (*Pax5* and *Fcmr*) as well as the responses of canonical pathways (Figures 4B and 4C). The results revealed that jejunal immunity of the CAS-fed groups was oriented toward pro-inflammatory responses, whereas the WPI-fed groups showed a reduction in inflammation.

High WPI improved the liver transcriptome affected by CAS-associated HFLC

Most of the differences in lipid metabolism between CAS and WPI were observed at 55% fat (Table S3). Expression of genes involved in lipogenesis was downregulated, and genes associated with fatty acid (FA) β-oxidation were upregulated in WPI with 40% and 55% fat relative to corresponding CAS groups, where most of the differences were observed at 55% fat (Figures 5A and 5B). Similar differential effects were observed on mRNA levels of regulators of FA synthesis and β-oxidation; namely, the upstream regulator CHREBP (carbohydrate-response element-binding protein) and STAT5B (Figures 4B and S3A). Furthermore, feeding WPI in the 55% dietary fat group showed increased activity of catabolic pathways, such as ketogenesis and tryptophan degradation, relative to feeding CAS and 55% fat (Figure S3B).

Striking differences in hepatic expression of genes involved in inflammation were observed between CAS and WPI at 40% and 55% fat, in line with the lipid transcriptome. In CAS-fed animals, intake of 40% and 55% fat increased expression of cytokines, chemokines, ILs, and other inflammatory markers and activated pro-inflammatory upstream regulators/pathways (LPS- and IL-related signaling, etc.) and downregulated the anti-inflammatory regulator HNF4A (Figures 5C, S3A, and S3B). In contrast, expression of liver inflammation markers and activity of regulators/pathways was largely unaffected by increasing fat in WPI-fed animals. The WPI and 55% fat-fed group showed reduced expression of genes involved in hepatic inflammation and inhibition of pro-inflammatory regulators/pathways relative to the CAS 55% fat group. In particular, the MYD88 causal network was inhibited in WPI-fed mice relative to CAS-fed mice at 55% dietary fat (Figure S2G).

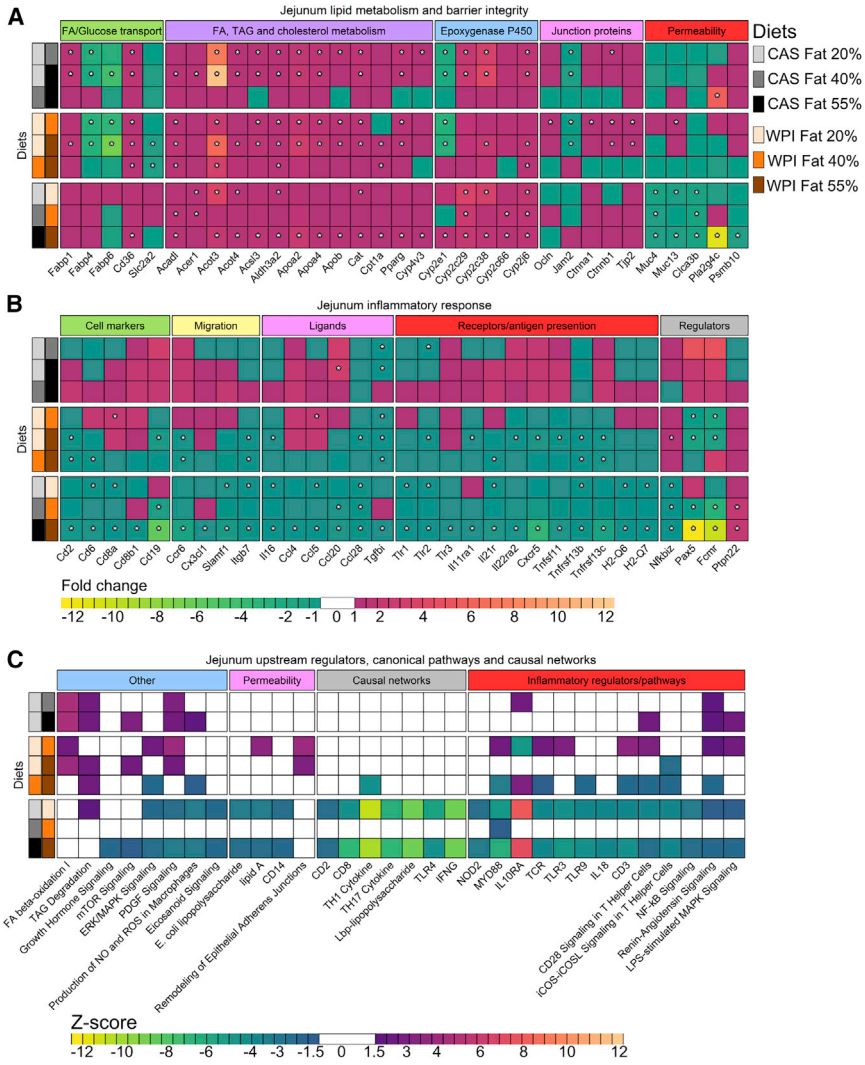

Figure 4. Jejunal transcriptome response to 30% protein with variable fat and protein types

(A and B) The expression of genes involved in lipid metabolism and intestinal barrier function (A) and inflammatory pathways (B). The values are represented as log2 fold changes between corresponding diets. *$p < 0.05$.

(C) Heatmap derived from IPA, showing significant changes ($p < 0.05$) in selected causal networks, upstream regulators, and canonical pathways with activation *Z* scores higher than 1.5 (activation) or lower than −1.5 (inhibition). White cells indicate insignificant changes in the selected pathways/regulators. n = 11–12 biologically independent samples. See Table S4 for IPA statistics and pathway/regulator target molecules.

Upstream regulators/canonical pathways associated with disease progression, including hepatic fibrosis and type II diabetes mellitus signaling, were activated with increasing fat in CAS-fed animals (20% versus 40% and 20% versus 55% fat), and activation of these regulators/pathways was not observed in WPI-fed animals (Figures S3A and S3B). The reduction of liver weight in WPI relative to CAS at 40% and 55% fat (Figure 3D) thus appeared to occur in parallel with a reduction of regulators associated with proliferation and cell cycle control of chromosome replication (Figure S3B), along with altered lipid metabolism, which together may underlie the reduced inflammatory response.

To assess whether the transcriptome data support lipid metabolism in the liver, a metabolomics analysis was undertaken. This showed that the livers of mice ingesting high WPI and 55% fat had reduced C16 and C20 monounsaturated FAs and polyunsaturated FAs, consistent with transcriptome data showing increased β-oxidation in WPI relative to CAS feeding (Figures 5B and S3C). Intriguingly, the 40% and 55% fat groups with WPI had higher levels of the very-long-chain FAs (VLCFAs) compared with the corresponding CAS groups (Figure S3C). The differences in VLCFA could be related to differences in processing of the VLCFAs into sphingolipids in the markedly differently sized livers of WPI- and CAS-fed mice. Notably, RICTOR (rapamycin-insensitive companion of mTOR), a component of mTORC2 involved in *de novo* lipogenesis, synthesis of sphingolipids, and development of liver steatosis (Guri et al., 2017), was upregulated in the CAS with 40% and 55% fat groups relative to the corresponding WPI groups (activation *Z* scores of 7 and 8 for HFD-CAS versus 2.5 and 3 for HFD-WPI) (Figures S3A; Table S4). Moreover, consistent with increased processing of VLCFA, the 40% and 55% fat with CAS diets showed activation of lactosylceramide-, sphingosine-1 phosphate-, and LDL (low-density lipoprotein)-related signaling and of sphingolipid synthetic/degradation genes alongside a reduction in the pool of VLCFAs relative to the corresponding WPI groups (Figures 5A, S3A, and S3B). These findings suggest that *de novo* sphingolipid synthesis is increased in hepatocytes of CAS-fed animals, likely leading to glucosylceramide accumulation. Given that the latter is a known stimulator of cell proliferation and tissue growth, these observations may explain the differences in liver weight and abundance of VLCFAs in the CAS and WPI groups.

In summary, analysis of the liver transcriptome revealed that intake of WPI impeded the negative effects of high-fat feeding (such as increased lipogenesis, inflammation, and activation of disease-related pathways), whereas intake of CAS exacerbated these effects.

Hypothalamic transcriptome responded to high WPI with high fat

In the hypothalamus, intake of 40% and 55% fat significantly increased the number of differentially expressed genes

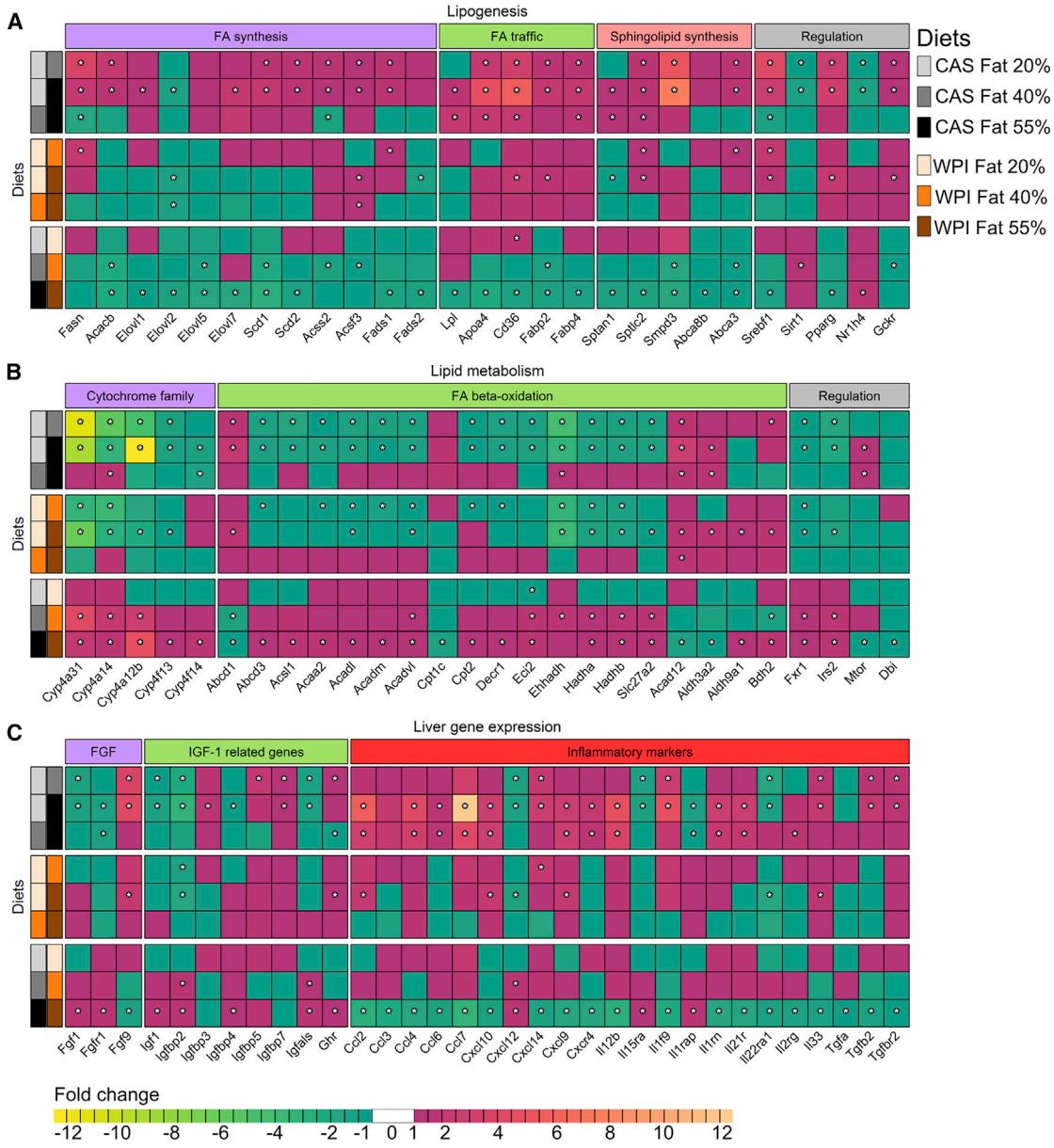

Figure 5. Hepatic expression of genes associated with lipid metabolism, fibroblast growth factor (FGF), and IGF-1 signaling for the 30% protein group with variable fat and protein types

(A–C) Heatmaps show the expression of genes involved in (A) *de novo* lipogenesis, (B) FA β-oxidation, and (C) cytochrome ω-hydroxylation of FAs and IGF-1/FGF-related genes. The values are represented as log2 fold changes between corresponding diets. *$p < 0.05$. n = 11–12 biologically independent samples. See Table S4 for IPA statistics and pathway/regulator target molecules.

compared with 20% fat (Table S3). The effect of protein quality on hypothalamic gene expression (CAS versus WPI) was only seen with the highest fat content (55%), where several changes in signaling pathways were seen in WPI relative to CAS. These include ghrelin receptor (*Ghsr*) and its associated pathways (G-αq and phospholipase C signaling) as well as increased oxidative phosphorylation (OXPHOS) and TCA (tricarboxylic acid cycle) cycle and decreased ROS (reactive oxygen species) production compared with mice fed CAS and 55% fat (Figures S4A and S4C). Upstream regulators (NFE2L2, PPARGC1A, and PPARGC1B) that activate expression of genes involved in OXPHOS were upregulated in mice fed WPI relative to those fed CAS at 55% fat (Figures S4B and S4D), which occurred alongside a reduction in IL and chemokine inflammatory pathways (Figures S4A and S4C). PTPs and Socs3 are negative regulators of insulin, IGF-1 and leptin signaling in the hypothalamus and other tissues (Arroba and Valverde, 2015; Cao et al., 2018; Shintani et al., 2017). Expression of the Socs3 gene and genes

from the PTP family and their related signaling (PTPRK and PTPRO [PTP receptor type K and O, respectively]) were downregulated in WPI relative to CAS at 55% fat (Figures S4A and S4B; Table S4). In line with this, insulin and IGF-1 receptor pathways (INSR [insulin receptor] and IGF1R) were upregulated in WPI compared with CAS (Figure S4B). In summary, the hypothalamic transcriptome revealed a reduction in hormone-associated signaling (leptin and insulin) and OXPHOS in CAS- but not WPI-fed animals at 55% fat.

High WPI increased microbial proteogenic and lipid metabolism pathways and changed cecal and fecal metabolites

To reveal the effect of 30% protein intake on the gut microbiome, shotgun metagenomic sequencing was applied to cecal content. At the species level, alpha diversity did not differ across the groups (Figure S5C). Similar results were obtained with respect to the alpha diversity of pathways (data not shown). In contrast, analysis of beta diversity revealed a significant separation between 30% CAS and WPI with respect to pathways and species at 40% and 55% fat (Figures 6A and S5A, respectively). Intake of CAS was associated with an increased relative abundance of *Bacteroides vulgatus*, whereas intake of WPI was accompanied by increased abundance of *Akkermansia muciniphila* and *Bacteroides uniformis* (Figure 6B). The proteinogenic amino acid degradation was higher in 30% WPI compared with CAS at 55% fat (Figure 6C). Furthermore, protein type differentially affected bacterial amino acid biosynthesis with lower valine and higher glutamate synthesis in WPI-fed relative to CAS-fed mice. Elevated amino acid degradation was coupled with increased lipid biosynthesis with higher production of unsaturated (oleate) and saturated (stearate) FAs in WPI-fed relative to CAS-fed mice at 40% and 55% dietary fat (Figure 6D). In contrast, CAS-fed groups showed an increase in sugar and polysaccharide degradation, pyruvate butanol fermentation, and alcohol degradation pathways and a reduction in pyruvate propanoate fermentation and acetate formation relative to WPI at 55% fat (Figure S5B; Table S5).

Metabolomics analysis of cecal content (40% and 55% fat groups only) revealed a clear separation between mice fed two 30% protein types (corrected Wilcoxon rank-sum test, $p < 0.001$ for CAS versus WPI at 40% and 55% fat) (Figure S6A), similar to the differences between CAS and WPI for bacterial pathways/species (Figures 6A and S5A). In line with increased bacterial amino acid catabolism, WPI-fed groups had lower levels of branched-chain amino acids (BCAAs) (leucine and valine) and dipeptides and higher levels of branched-chain FA (BCFA) (2,4-dimethylpimelic acid) in the cecum relative to CAS 40% and 55% fat-fed groups (Figures S6B and S6C). Notably, odd long-chain FAs (LCFAs) (C15:0 and C17:0), which were not present in the diets and could be produced from gut-derived propionic acid, were enhanced in the WPI-fed 55% fat group (Figure S5B). Moreover, many other metabolites linked to ROS production and apoptosis (Chao et al., 2019) (3,5-DMA [3,5-Dimethylaniline]), and liver cirrhosis (pipecolinic acid, a metabolite of lysine) (Kawasaki et al., 1988), were reduced (Figure S6D), whereas the levels of medium-chain dicarboxylic acids (MCDAs) were increased in WPI relative to CAS (Figure S6D). Azelaic acid possesses anti-inflammatory properties, suberic and sebacic acids are microbial metabolites formed from breakdown of oleic and linoleic FAs, and andrographolide is a known promoter of growth of *A. muciniphila* (Su et al., 2020), as seen in WPI-fed animals. Along with upregulation of microbial FA biosynthesis pathways, 30% WPI groups, with their potential to bind dietary fat, had increased fecal TAGs relative to CAS at 55% fat (Figure S6E).

Study 2: High WPI- and CAS-associated microbiota differentially affected weight gain

The biggest differences of host tissue transcriptomic responses and microbial taxonomic/functional diversity were detected when feeding 30% CAS and WPI at 55% fat (Figures 4, 5, 6, S4, and S5). Because this occurred when EI was similar between groups that had contrasting tissue effects, we selected these diets to study whether the functional potential of the microbiota can alter the host energy supply and, therefore, the host tissue responses (Figure 7A). First, in this study, similar to study 1, 20-week-old animals were fed for 4 weeks with CAS or WPI in a 55% fat diet and switched to a 4-week antibiotic (ABX) treatment (i.e., CAS-ABX or WPI-ABX), or they continued to receive the same diet (CAS-control, WPI-control). The fecal microbiota was analyzed before ABX treatment (time point 1 [T1]), after treatment (T2), in the middle of the 4-week fecal material transplantation (FMT) period (T3), and at the end of FMT (T4) (Figures 7 and S7; Tables S6 and S7).

Effect of ABX treatment

The BW gain of CAS-ABX and WPI-ABX was significantly lower than the gain of the corresponding control groups, where the effect of ABX treatment was stronger in WPI-fed animals (Figure 7B). The BW gain of control groups was not significantly different during this period, similar to the result of a corresponding period in a previous study (study 1; weeks 4–8, CAS = 4.7 ± 0.7 g, WPI = 5.1 ± 0.4 g; Figure 1C), as was the average EI for the same period in the two trials (Figure S7A). In study 2, WPI fed animals had slightly higher but not significant EI (Figure S7A). ABX treatment reduced the alpha diversity of species in the CAS and WPI groups and changed the microbial composition at the genus level, resulting in dominance of *Escherichia* in CAS and increased abundance of *Chryseobacterim* and *Escherichia* in WPI (Figures 7D and 7E). ABX treatment reduced pathways associated with energy metabolism (e.g., pyruvate acetate fermentation), sugar/polysaccharide degradation, and CHO/lipid biosynthesis more in the WPI-ABX group than in the CAS-ABX group (Figure 7F). Proteinogenic amino acid degradation was abolished completely in the WPI- and CAS-ABX groups (Table S7).

Effect of FMT intervention (T3 and T4)

The WPI group with CAS microbiota (WPI-FMT) gained less weight than the WPI control group after 2 weeks of FMT (Figure 7C; T3). The opposite result was observed during the subsequent 2 weeks of FMT, with higher BW gain in WPI-FMT relative to the WPI control group (Figure 7C; T4). This suggested that the CAS microbiota overrode the initial WPI diet effects on host BW gain, leading to increased BW gain at the end of the FMT period. The BW gain of the CAS group receiving the WPI microbiota (CAS-FMT) did not change after 2 weeks of FMT compared with the start point of fecal transfer (RM [repeated measures]

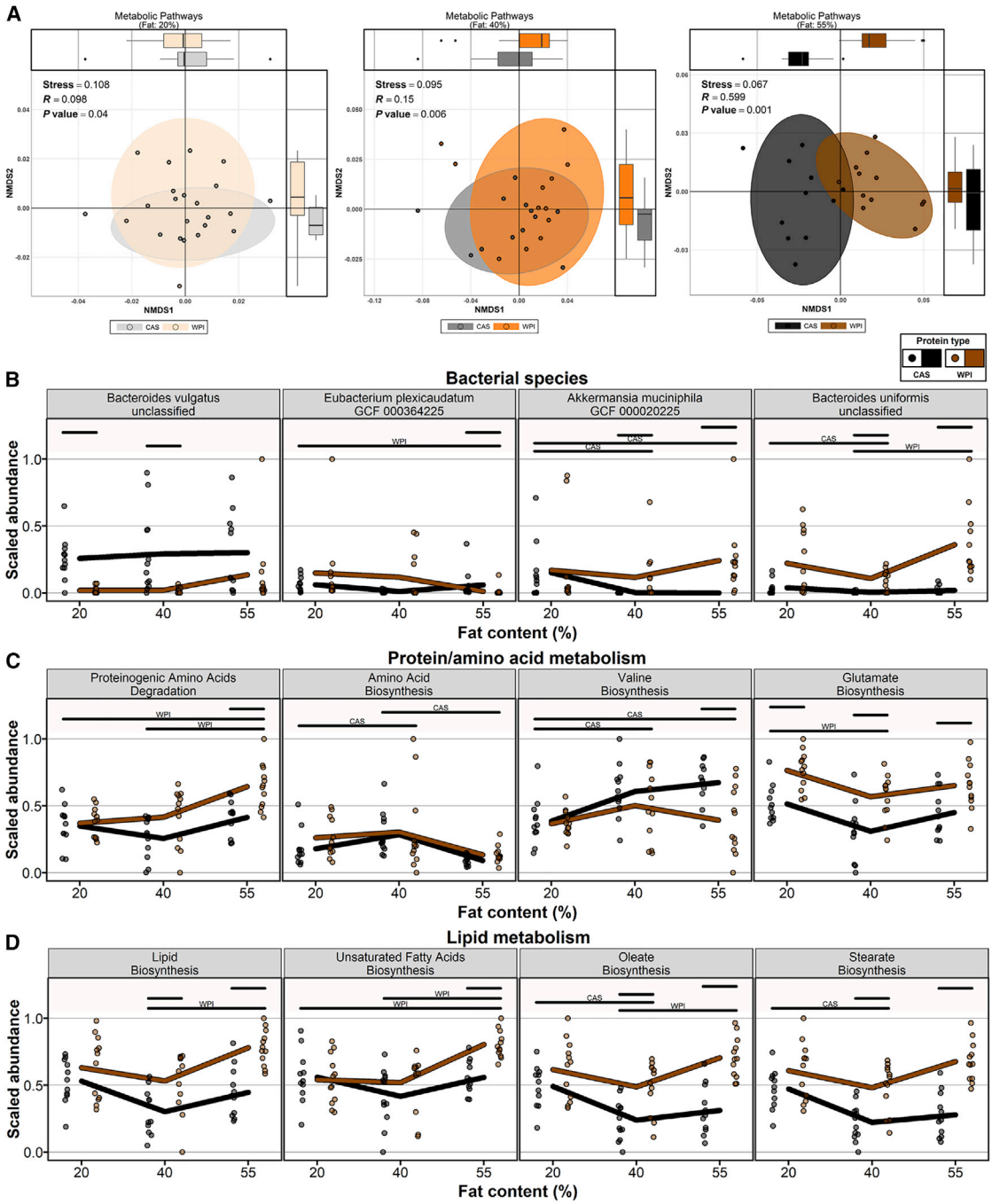

Figure 6. Effects of 30% protein diets on the cecal microbiome

(A) Ordination of metabolic pathways for both protein types at 20%, 40%, and 55% fat. Group separation becomes more pronounced as fat content increases. (B–D) Variation of (B) selected bacterial species, (C) protein/amino acid metabolism, and (D) lipid metabolism pathways according to protein type and fat percentage. Solid bars indicate significance (adjusted Wilcoxon rank-sum test, $p < 0.05$). Within-protein-group comparisons are indicated by WPI or CAS, whereas cross-group differences for fat percentage are indicated by blank bars. n = 11–12 biologically independent samples. See Figure S5 and Table S5 for variation of other microbial metabolism pathways according to protein type and fat percentage.

ANOVA, $p = 1$) and became significantly lower than the BW gain of CAS-control (Figure 7C; T3). This suggested that the WPI microbiota was able to initially impede the effects of the CAS diet on host weight gain (2 weeks). In contrast, after an additional 2 weeks of FMT, the BW gain of the CAS-FMT group increased significantly (RM ANOVA, $p = 0.0002$) to the level of the CAS control group (Figure 7C; T4). This suggested that prolonged CAS intake overrode the effect of the WPI microbiota seen initially.

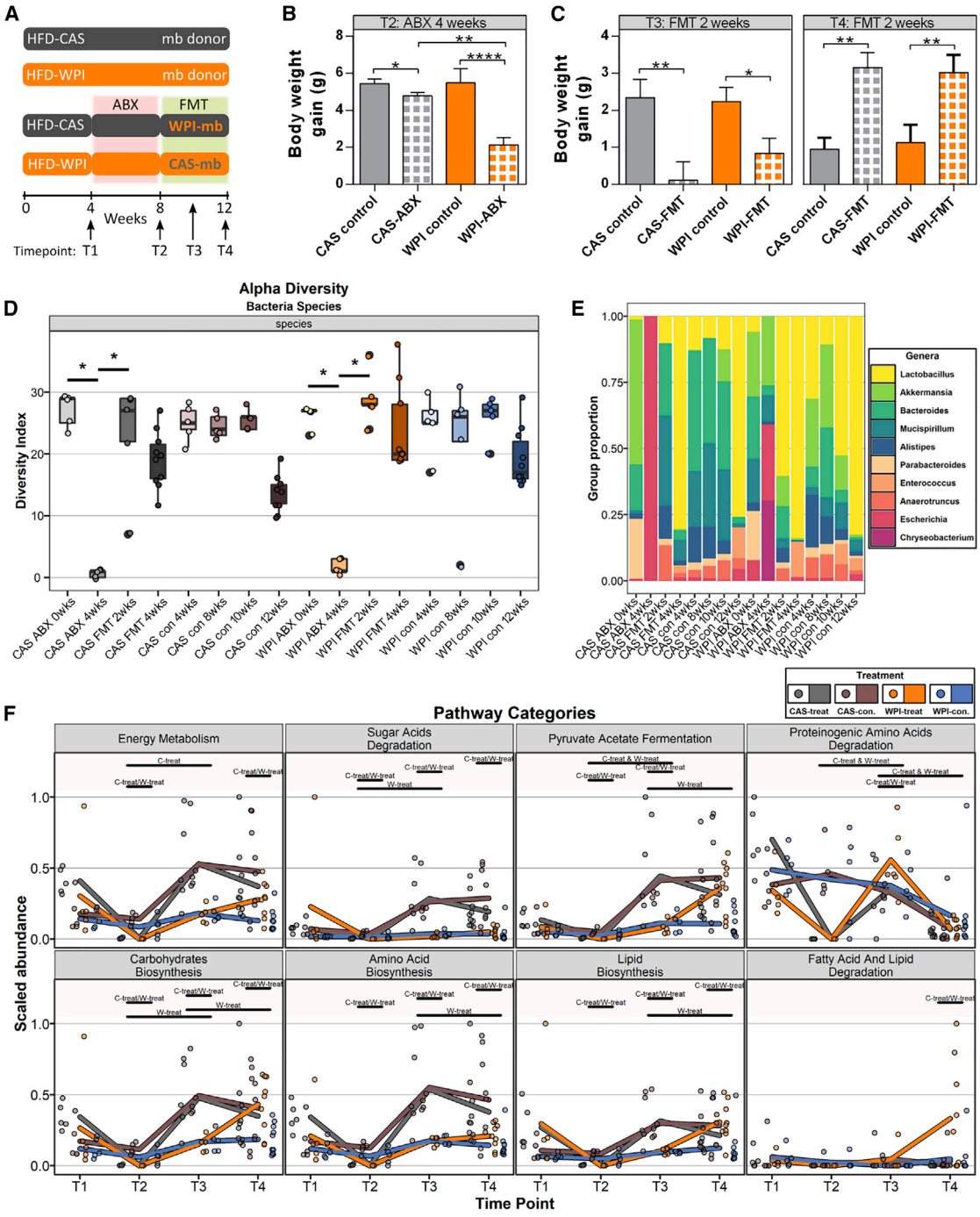

Figure 7. The effect of the gut microbiota on BW gain in animals fed 55% fat CAS or WPI

(A) Design of the ABX/FMT experiment.

(B and C) BW gain changes during the ABX (B) and FMT (C) experiment.

(D) Alpha diversity for species.

(E) Bacterial composition of the different communities at the genus level.

(F) Selected metabolic pathways. Group comparisons are indicated by the following abbreviations: C-treat, CAS treatment; W-treat, WPI treatment. C-treat/W-treat, comparison between treatment groups; C-treat & W-treat, comparison across time points. *$p < 0.05$, **$p < 0.01$, ***$p < 0.001$, ****$p < 0.0001$. n = 9–10 biologically independent samples. See Table S7 for variation of microbial metabolism pathways according to protein type and time point of treatment. For bioinformatic analysis, the fecal samples were collected per cage at T1–T3 and from individual animals at T4 with 5 (T1–T3) and 9–10 (T4) biologically independent samples.

The FMT restored alpha diversity in CAS and WPI to the level of the corresponding control groups (Figure 7D). The abundance of *Lactobacillus*, *Bacteroides*, and *Mucispirillum* increased during the first 2 weeks of FMT in the CAS and WPI-FMT groups (Figures 7E and S7D). A further 2 weeks of FMT reduced the abundance of *Bacteroides* and *Mucispirillum* and increased *Lactobacillus* in WPI relative to CAS (Figure S7D). In particular, the WPI-FMT group had a higher relative abundance of *Lactobacillus reuteri* (*L. reuteri*) relative to CAS-FMT group at T4. The beta diversity of pathways/species was not significantly different between the CAS- and WPI-FMT groups at T3; neither group gained BW (Table S6; Figure S7C).

Focusing on pathways, the effect of ABX on proteinogenic amino acid degradation and lipid biosynthesis was reversed after 2 weeks of FMT; the WPI- and CAS-FMT groups had a similar abundance of these pathways at T3 (Figure 7F), when the BW gain in the CAS-FMT group was lower than in the CAS controls, and where WPI-FMT was even lower than WPI-control (Figure 7C). Both pathways decreased in the CAS-FMT group (receiving the WPI microbiome) from T3 to T4 to the level of CAS-control, and, at the same time, the BW gain of the CAS-FMT group matched that of the CAS controls. In line with a suggestion that proteogenic amino acid degradation pathways and lipid biosynthesis pathways are needed for WPI microbiota to affect weight gain, when proteinogenic amino acid degradation was reduced from T3 to T4 in the WPI-FMT group (Figure 7F), presumably because of the competing transplanted CAS microbiota in the WPI-FMT group, the weight gain of the WPI-FMT group increased relative to the WPI-control group (Figure 7C; T4).

DISCUSSION

Contrary to the popular view that high protein intake prevents the unhealthy metabolic outcomes of a high-fat diet, we found that the effects of dietary fat depends on an interaction between protein quantity and quality. Although increasing dietary fat increased BW gain and tissue weight irrespective of protein quantity and source in adult mice, this increase was accentuated when high (30%) CAS was used and was impeded by (30%) WPI, and this specific effect was observed only in the 40% and 55% dietary fat-fed groups that had proportionally reduced CHO (HFLC diets).

In agreement with a recent study (Hu et al., 2018), HFDs increased EI and high-protein (30%) diets did not reduce intake, contrasting predictions of the protein leverage hypothesis (Simpson and Raubenheimer, 2005). Strikingly, 30% WPI reduced EI relative to 30% CAS (with 40% fat) during the first 6 weeks of the study (half of the entire treatment period). Interestingly, the reduction in EI in the WPI group affected BW gain only at the end of the 6-week period, and the reduced BW gain then progressed even after EI normalized in the WPI group, leading to reduced AT weight and lower hormone (e.g., leptin) (McAllan et al., 2013) and glucose levels in the plasma. Given that the 30% WPI group had an altered microbiota composition and functional pathways at the end of the study, we propose that an unique interaction between EI and microbiota arose in WPI and 40% fat-fed mice during diet intake that allowed the animals to continue to gain less weight with support of an active microbial component and even in the absence of the EI component beyond week 6.

In line with the above suggestion, intake of 30% WPI and 55% dietary fat caused mice to have an EI similar to animals fed CAS with matching protein, fat, and CHO quantities, but they still gained less weight and had distinct microbiota composition and functional pathways. These differences were reflected in the growth-related signal IGF-1, where the reduced IGF-1 hormone level correlated with BW gain and tissue weight with WPI intake. The responding tissues were AT depots, pelage, liver, and organs of the digestive tract (the small intestine and colon), and WPI fed mice still had much higher plasma TAG levels. Interestingly, similar opposing responses of IGF-1 and plasma TAG level have been observed in humans fed CAS and WPI (Hoppe et al., 2009, 2004; Mariotti et al., 2015). This suggested energy deposition and use in tissues in proportion to circulating levels of growth signal (IGF-1) with WPI despite an EI similar to CAS-fed mice. Beyond the difference in IGF-1 and TAG response, several other pieces of evidence support the suggestion that the similar EI is supplied differently to tissues in mice fed WPI compared with CAS.

First, the liver transcriptome revealed genes involved in FA/lipid uptake and synthesis to be upregulated and genes involved in FA/lipid degradation to be downregulated following a proportional increase in dietary fat (20% to 55%) in 30% CAS-fed animals, similar to ectopic fat deposition in the liver, and development of insulin resistance and liver disease, whereas these molecular signatures were absent in the WPI group at 55% fat. This was reflected in the increased liver weight in CAS- but not WPI-fed animals.

The second piece of evidence relates to the inflammatory response, which indicated tissue damage when cell growth was not matched to energy supply and deposition. The transcriptome analysis showed that WPI reduced the inflammatory response in the hypothalamus, liver, and jejunum, whereupon improvements in insulin and IGF-1 receptor signaling (in the hypothalamus) occurred, alongside downregulation of the PTPRJ (PTP receptor type J) pathway and recoupling of the GH and IGF-1 axis. Moreover, WPI protected intestinal integrity during high-fat feeding by upregulation of genes encoded junctional proteins, *Ptpn22* and the IL-10RA regulator known to be involved in maintenance of intestinal integrity and homeostasis (Spalinger et al., 2015) and by increased production of andrographolide in the cecum, which is known to improve intestinal permeability and mucosal architecture and reduce NAFLD (non-alcoholic fatty liver disease) (Shi et al., 2020). These effects were further supported by inhibition of LPS- and MYD88-related transcriptome signaling, linked to reduced liver fat accumulation and inflammation (Cani et al., 2008), reduced plasma TNF-α/CCL2 levels, and reduced NF-κB and LPS/TLR4 activation in tissues (Ahmad et al., 2018). The additional reduction of plasma IL-15 and IP-10 cytokines and transcriptomics profile of responding immune cells in the jejunum (CD2, CD8, Th1, and Th17; Figure 4C) and liver (CD44; Figure S3A) support a link between intestinal T cell density and systemic inflammation and markers of liver alterations (Monteiro-Sepulveda et al., 2015).

The third piece of evidence supporting a mismatch between energy supply and deposition (and inflammatory response) in

30% WPI and 55% fat-fed mice relates to the response of the gastrointestinal tract, which showed consistently reduced weights of the stomach, intestine, and colon, with transcriptomics data from the jejunum showing a fewer markers of immune cells and higher expression of somatostatin receptor 1, which is known to reduce proliferation of intestinal cells (Modarai et al., 2016) compared with CAS-fed mice. These data, coupled with increased cecal availability of LCFAs and fecal TAGs and a human study showing that WPI intake reduced fat absorption through the intestine compared with CAS intake (Stanstrup et al., 2014) and a murine study showing increased fat excretion (Pilvi et al., 2007), suggested fecal energy loss with 30% WPI intake. Elevated TAG and FA excretion in the WPI group could be due to a reduction of gut capacity and associated changes in digestion and absorption of fat. It could also be due to the known fat-binding properties of whey proteins (Jeewanthi et al., 2015), with the exception of cecal BCFAs and LCFAs (C15:0 and C17:0), which were detected in higher abundance in the cecum in the high-WPI group, presumably produced by bacteria (see below). Previous work reported that these LCFAs were inversely correlated with type 2 diabetes and cardiovascular disease (Pfeuffer and Jaudszus, 2016).

Reducing tissue expansion with accumulation of ectopic fat is difficult, but evidence suggests that one way to achieve this might be to target the gut microbiota (Koutnikova et al., 2019) and alter the dietary nutrient supply reaching the host. WPI is a rich source of essential amino acids (EAAs) and BCAAs, and because BCFAs are derived from BCAAs and produced/utilized by several *Lactobacillus* and *Bacillus* species, it was intriguing that high (30%) WPI with 55% fat-fed mice had increased bacterial proteinogenic amino acid degradation and increased lipid/FA biosynthesis pathways. This functional change in the WPI microbiota was associated with reduced cecal levels of several amino acids and increased levels of cecal LCFAs in the WPI groups alongside elevated BCFAs, heightened levels of which have been linked previously to reduced enterocolitis via upregulation of the anti-inflammatory IL-10 cytokine (Ran-Ressler et al., 2011). Thus, by modifying the host dietary nutrient supply, with little capacity to absorb through the lower part of the gut (e.g., LCFA), the WPI sensitive microbiota may be contributing to the (fecal TAG-related) energy loss in WPI-fed mice reported previously and captured here. We cannot also exclude the possibility that there may be a parallel effect of microbiota-induced change in nutrient supply affecting tissue metabolism differently in protein groups. In support of this, although the FA profile and liver transcriptome supported accumulation of fat and growth of the liver in CAS, when WPI-fed mice had a reduced response, EAT appeared to respond in an opposite way in terms of weight and gene expression, whereas SAT was unresponsive. Diet-induced changes in the functional repertoire of the studied microbiota may be due to selective growth of specific species. For example, WPI intake increased the abundance of cecal *B. uniformis* and *A. muciniphila*, both of which have been shown to alleviate immunological and metabolic dysfunction in mice with HFD-induced obesity (Everard et al., 2013; Gauffin Cano et al., 2012). In further support of a link between diet, microbiota, and host metabolic responses, a recent study by Ruocco et al. (2020) showed that a designer diet in which CAS-derived amino acids were substituted with a mixture of EAAs could prevent and reverse obesity in mice. In agreement with our study, the metabolic effects of EEA-rich diets were achieved independent of EI and were dependent on the gut microbiota changes.

Our investigation with ABX and FMT intervention confirmed the functional potential of the microbiota to modify the nutrient accessibility to the hosts fed 55% fat and 30% CAS or WPI. Notably, during the first 2 weeks of FMT (T2–T3), WPI-derived microbiota reduced BW gain and increased proteogenic amino acid degradation and lipid biosynthesis in the recipient CAS (CAS-FMT) group and the abundance of these pathways was reduced by the end of FMT period, whereupon BW was regained. This suggests that continual ingestion of the CAS diet overrode the initial effects of WPI microbiota supplementation and that the presence of WPI-derived nutrients such as BCAAs may be required to maintain the functional and composition effects of the associated gut microbiota. In line with this suggestion, CAS-derived microbiota also did not increase the BW gain of the WPI-ingesting FMT group during the first 2 weeks of the FMT period, when this group had increased proteinogenic amino acid degradation and lipid/FA biosynthesis pathways. However, when the AA degradation pathway was reduced by the end of the FMT period and lipid/FA biosynthesis increased during the same period in the WPI-FMT group, presumably because of the competition in the WPI-FMT group receiving the CAS microbiota, the lack of activity in one pathway was associated with significant weight regain in the WPI-FMT group, higher than the weight gain in WPI controls. It is noteworthy that the WPI group (WPI-FMT) receiving the CAS microbiota increased the abundance of *Lactobacillus* genera and *L. reuteri*, which are known to have anti-obesity effects on the host (Choi et al., 2020), where *L. reuteri* attenuated HFD-induced BW gain via IL-10-mediated induction of lymphocytes and restoration of the T-regulatory/Th17 cell balance in the intestine (Poutahidis et al., 2013).

These results suggest a model where the HFLC diet combined with high CAS protein promoted BW gain via increased nutrients coming through the gut, which, in turn, triggered low-grade inflammation and tissue expansion, promoting metabolic dysfunction, which is driven by a CAS-associated unhealthy gut microbiota. In contrast, the HFLC diet combined with high WPI impeded BW gain by modifying host accessibility to nutrients in the gut, achieved by reducing gut size and promoting growth of a healthy microbiota, allowing the host to stay metabolically healthier. The data highlight the importance of selecting proteins rich in essential amino acids for improving the metabolic outcomes of a high-fat diet.

Limitations of study

Although we used over 200 animals in our study and compiled over 100 observations per animal, our study has limitations. The experiments were performed in male mice during a specific age (early adulthood), using 2 protein sources in a single combination of saturated and unsaturated FAs and one source of fiber. This contrasts with human nutrition, but our data provide an incentive for further investigation with different dietary combinations and added measurements of tissue morphology and cellular behavior (beyond what was shown here). Moreover, and despite the fact that our study demonstrated the interaction

between specific dietary proteins and microbiotas in regulating BW, additional work is necessary to identify a mechanical link between specific dietary components, microbiotas, and tissue metabolic effects.

STAR★METHODS

Detailed methods are provided in the online version of this paper and include the following:

- KEY RESOURCES TABLE
- RESOURCE AVAILABILITY
  - Lead contact
  - Materials availability
  - Data and code availability
- EXPERIMENTAL MODEL AND SUBJECT DETAILS
  - Mice
  - Study 1
  - Study 2
- METHOD DETAILS
  - RNA extraction, transcriptome analysis and qPCR
  - Plasma metabolites and hormones
  - Cecal and fecal microbiome
  - Metabolomics of cecal content
  - Liver fatty acid analysis
- QUANTIFICATION AND STATISTICAL ANALYSIS

SUPPLEMENTAL INFORMATION

Supplemental information can be found online at https://doi.org/10.1016/j.celrep.2021.109093.

ACKNOWLEDGMENTS

This work was supported by a research grant from Science Foundation Ireland (SFI) under grant SFI/16/BBSRC/3389, BBSRC under grant number BB/P009875/1 (to K.N.N. and J.R.S.), and in part by SFI and the Department of Agriculture, Food and Marine under grant 16/RC/3835 (to VistaMilk). We thank Conall Strain, David Mannion, and John Leech for contributing to the metabolomics analysis. We thank Alina Kondrashina for help with the Milliplex system.

AUTHOR CONTRIBUTIONS

K.N.N., O.N., and J.R.S. designed the experiments. O.N., K.N.N., Y.P., S.B., D.D., Á.F., X.Y., and A.M.R. conducted the experiments. W.B. and O.N. developed and performed bioinformatics and analysis of RNA-seq and the microbiome. O.N., W.B., T.F.S.B., J.G., A.W., L.B., L.G., P.C., S.M., P.D.C., L.M., S.M., S.E.M., J.F.C., L.C., J.W., and J.R.S. collected data and assisted with data analyses. L.G. provided essential equipment. O.N. and K.N.N. co-wrote the manuscript. J.R.S., P.D.C., and W.B. revised the manuscript.

DECLARATION OF INTERESTS

The authors declare no competing interests.

Received: November 20, 2020
Revised: March 8, 2021
Accepted: April 16, 2021
Published: May 11, 2021

REFERENCES

Abete, I., Astrup, A., Martínez, J.A., Thorsdottir, I., and Zulet, M.A. (2010). Obesity and the metabolic syndrome: role of different dietary macronutrient distribution patterns and specific nutritional components on weight loss and maintenance. Nutr. Rev. *68*, 214–231.

Ahmad, R., Al-Roub, A., Kochumon, S., Akther, N., Thomas, R., Kumari, M., Koshy, M.S., Tiss, A., Hannun, Y.A., Tuomilehto, J., et al. (2018). The Synergy between Palmitate and TNF-α for CCL2 Production Is Dependent on the TRIF/IRF3 Pathway: Implications for Metabolic Inflammation. J. Immunol. *200*, 3599–3611.

Altunkaynak, B.Z., Ozbek, E., and Altunkaynak, M.E. (2007). A stereological and histological analysis of spleen on obese female rats, fed with high fat diet. Saudi Med. J. *28*, 353–357.

Archer, E., Pavela, G., McDonald, S., Lavie, C.J., and Hill, J.O. (2018). Cell-Specific "Competition for Calories" Drives Asymmetric Nutrient-Energy Partitioning, Obesity, and Metabolic Diseases in Human and Non-human Animals. Front. Physiol. *9*, 1053.

Arroba, A.I., and Valverde, Á.M. (2015). Inhibition of protein tyrosine phosphatase 1B improves IGF-I receptor signaling and protects against inflammation-induced gliosis in the retina. Invest. Ophthalmol. Vis. Sci. *56*, 8031–8044.

Berryman, C.E., Lieberman, H.R., Fulgoni, V.L., 3rd, and Pasiakos, S.M. (2018). Protein intake trends and conformity with the Dietary Reference Intakes in the United States: analysis of the National Health and Nutrition Examination Survey, 2001-2014. Am. J. Clin. Nutr. *108*, 405–413.

Bolger, A.M., Lohse, M., and Usadel, B. (2014). Trimmomatic: a flexible trimmer for Illumina sequence data. Bioinformatics *30*, 2114–2120.

Brun, P., Castagliuolo, I., Di Leo, V., Buda, A., Pinzani, M., Palù, G., and Martines, D. (2007). Increased intestinal permeability in obese mice: new evidence in the pathogenesis of nonalcoholic steatohepatitis. Am. J. Physiol. Gastrointest. Liver Physiol. *292*, G518–G525.

Buchan, L., St Aubin, C.R., Fisher, A.L., Hellings, A., Castro, M., Al-Nakkash, L., Broderick, T.L., and Plochocki, J.H. (2018). High-fat, high-sugar diet induces splenomegaly that is ameliorated with exercise and genistein treatment. BMC Res. Notes *11*, 752.

Caballero, B. (2007). The global epidemic of obesity: an overview. Epidemiol. Rev. *29*, 1–5.

Cani, P.D., Bibiloni, R., Knauf, C., Waget, A., Neyrinck, A.M., Delzenne, N.M., and Burcelin, R. (2008). Changes in gut microbiota control metabolic endotoxemia-induced inflammation in high-fat diet-induced obesity and diabetes in mice. Diabetes *57*, 1470–1481.

Cao, L., Wang, Z., and Wan, W. (2018). Suppressor of cytokine signaling 3: Emerging role linking central insulin resistance and Alzheimer's disease. Front. Neurosci. *12*, 417.

Chao, M.W., Kuo, H.C., Tong, S.Y., Yang, Y.S., Chuang, Y.C., and Tseng, C.Y. (2019). In Vitro and In Vivo Analysis of the Effects of 3,5-DMA and Its Metabolites in Neural Oxidative Stress and Neurodevelopmental Toxicity. Toxicol. Sci. *168*, 405–419.

Choi, W.J., Dong, H.J., Jeong, H.U., Ryu, D.W., Song, S.M., Kim, Y.R., Jung, H.H., Kim, T.H., and Kim, Y.H. (2020). Lactobacillus plantarum LMT1-48 exerts anti-obesity effect in high-fat diet-induced obese mice by regulating expression of lipogenic genes. Sci. Rep. *10*, 869.

Dobin, A., Davis, C.A., Schlesinger, F., Drenkow, J., Zaleski, C., Jha, S., Batut, P., Chaisson, M., and Gingeras, T.R. (2013). STAR: ultrafast universal RNA-seq aligner. Bioinformatics *29*, 15–21.

Everard, A., Belzer, C., Geurts, L., Ouwerkerk, J.P., Druart, C., Bindels, L.B., Guiot, Y., Derrien, M., Muccioli, G.G., Delzenne, N.M., et al. (2013). Cross-talk between Akkermansia muciniphila and intestinal epithelium controls diet-induced obesity. Proc. Natl. Acad. Sci. USA *110*, 9066–9071.

Flegal, K.M., Kit, B.K., Orpana, H., and Graubard, B.I. (2013). Association of all-cause mortality with overweight and obesity using standard body mass index categories: a systematic review and meta-analysis. JAMA *309*, 71–82.

Franzosa, E.A., McIver, L.J., Rahnavard, G., Thompson, L.R., Schirmer, M., Weingart, G., Lipson, K.S., Knight, R., Caporaso, J.G., Segata, N., and Huttenhower, C. (2018). Species-level functional profiling of metagenomes and metatranscriptomes. Nat. Methods *15*, 962–968.

Gauffin Cano, P., Santacruz, A., Moya, Á., and Sanz, Y. (2012). Bacteroides uniformis CECT 7771 ameliorates metabolic and immunological dysfunction in mice with high-fat-diet induced obesity. PLoS ONE *7*, e41079.

Gorissen, S.H.M., Crombag, J.J.R., Senden, J.M.G., Waterval, W.A.H., Bierau, J., Verdijk, L.B., and van Loon, L.J.C. (2018). Protein content and amino acid composition of commercially available plant-based protein isolates. Amino Acids *50*, 1685–1695.

Gortner, W.A. (1975). Nutrition in the United States, 1900 to 1974. Cancer Res. *35*, 3246–3253.

Gu, Z., Eils, R., and Schlesner, M. (2016). Complex heatmaps reveal patterns and correlations in multidimensional genomic data. Bioinformatics *32*, 2847–2849.

Guri, Y., Colombi, M., Dazert, E., Hindupur, S.K., Roszik, J., Moes, S., Jenoe, P., Heim, M.H., Riezman, I., Riezman, H., and Hall, M.N. (2017). mTORC2 Promotes Tumorigenesis via Lipid Synthesis. Cancer Cell *32*, 807–823.e12.

Hall, W.L., Millward, D.J., Long, S.J., and Morgan, L.M. (2003). Casein and whey exert different effects on plasma amino acid profiles, gastrointestinal hormone secretion and appetite. Br. J. Nutr. *89*, 239–248.

Hamilton, C.C., and Anderson, J.W. (1992). Fiber and weight management. J. Fla. Med. Assoc. *79*, 379–381.

Hoppe, C., Mølgaard, C., Juul, A., and Michaelsen, K.F. (2004). High intakes of skimmed milk, but not meat, increase serum IGF-I and IGFBP-3 in eight-year-old boys. Eur. J. Clin. Nutr. *58*, 1211–1216.

Hoppe, C., Mølgaard, C., Dalum, C., Vaag, A., and Michaelsen, K.F. (2009). Differential effects of casein versus whey on fasting plasma levels of insulin, IGF-1 and IGF-1/IGFBP-3: results from a randomized 7-day supplementation study in prepubertal boys. Eur. J. Clin. Nutr. *63*, 1076–1083.

Hu, S., Wang, L., Yang, D., Li, L., Togo, J., Wu, Y., Liu, Q., Li, B., Li, M., Wang, G., et al. (2018). Dietary Fat, but Not Protein or Carbohydrate, Regulates Energy Intake and Causes Adiposity in Mice. Cell Metab. *28*, 415–431.e4.

Hu, S., Wang, L., Togo, J., Yang, D., Xu, Y., Wu, Y., Douglas, A., and Speakman, J.R. (2020). The carbohydrate-insulin model does not explain the impact of varying dietary macronutrients on the body weight and adiposity of mice. Mol. Metab. *32*, 27–43.

Jeewanthi, R.K., Lee, N.K., and Paik, H.D. (2015). Improved Functional Characteristics of Whey Protein Hydrolysates in Food Industry. Han-gug Chugsan Sigpum Hag-hoeji *35*, 350–359.

Johnsen, L.G., Skou, P.B., Khakimov, B., and Bro, R. (2017). Gas chromatography - mass spectrometry data processing made easy. J. Chromatogr. A *1503*, 57–64.

Kakimoto, P.A., and Kowaltowski, A.J. (2016). Effects of high fat diets on rodent liver bioenergetics and oxidative imbalance. Redox Biol. *8*, 216–225.

Kawasaki, H., Hori, T., Nakajima, M., and Takeshita, K. (1988). Plasma levels of pipecolic acid in patients with chronic liver disease. Hepatology *8*, 286–289.

Koutnikova, H., Genser, B., Monteiro-Sepulveda, M., Faurie, J.M., Rizkalla, S., Schrezenmeir, J., and Clément, K. (2019). Impact of bacterial probiotics on obesity, diabetes and non-alcoholic fatty liver disease related variables: a systematic review and meta-analysis of randomised controlled trials. BMJ Open *9*, e017995.

Li, B., Li, L., Li, M., Lam, S.M., Wang, G., Wu, Y., Zhang, H., Niu, C., Zhang, X., Liu, X., et al. (2019). Microbiota Depletion Impairs Thermogenesis of Brown Adipose Tissue and Browning of White Adipose Tissue. Cell Rep. *26*, 2720–2737.e5.

Lin, R., Liu, W., Piao, M., and Zhu, H. (2017). A review of the relationship between the gut microbiota and amino acid metabolism. Amino Acids *49*, 2083–2090.

Love, M.I., Huber, W., and Anders, S. (2014). Moderated estimation of fold change and dispersion for RNA-seq data with DESeq2. Genome Biol. *15*, 550.

Ludwig, D.S., Hu, F.B., Tappy, L., and Brand-Miller, J. (2018). Dietary carbohydrates: role of quality and quantity in chronic disease. BMJ *361*, k2340.

Mao, J., Hu, X., Xiao, Y., Yang, C., Ding, Y., Hou, N., Wang, J., Cheng, H., and Zhang, X. (2013). Overnutrition stimulates intestinal epithelium proliferation through β-catenin signaling in obese mice. Diabetes *62*, 3736–3746.

Mariotti, F., Valette, M., Lopez, C., Fouillet, H., Famelart, M.H., Mathé, V., Airinei, G., Benamouzig, R., Gaudichon, C., Tomé, D., et al. (2015). Casein Compared with Whey Proteins Affects the Organization of Dietary Fat during Digestion and Attenuates the Postprandial Triglyceride Response to a Mixed High-Fat Meal in Healthy, Overweight Men. J. Nutr. *145*, 2657–2664.

McAllan, L., Keane, D., Schellekens, H., Roche, H.M., Korpela, R., Cryan, J.F., and Nilaweera, K.N. (2013). Whey protein isolate counteracts the effects of a high-fat diet on energy intake and hypothalamic and adipose tissue expression of energy balance-related genes. Br. J. Nutr. *110*, 2114–2126.

McAllan, L., Speakman, J.R., Cryan, J.F., and Nilaweera, K.N. (2015). Whey protein isolate decreases murine stomach weight and intestinal length and alters the expression of Wnt signalling-associated genes. Br. J. Nutr. *113*, 372–379.

McManus, B.L., Korpela, R., Speakman, J.R., Cryan, J.F., Cotter, P.D., and Nilaweera, K.N. (2015). Bovine serum albumin as the dominant form of dietary protein reduces subcutaneous fat mass, plasma leptin and plasma corticosterone in high fat-fed C57/BL6J mice. Br. J. Nutr. *114*, 654–662.

Mitchell, S.E., Tang, Z., Kerbois, C., Delville, C., Konstantopedos, P., Bruel, A., Derous, D., Green, C., Aspden, R.M., Goodyear, S.R., et al. (2015). The effects of graded levels of calorie restriction: I. impact of short term calorie and protein restriction on body composition in the C57BL/6 mouse. Oncotarget *6*, 15902–15930.

Modarai, S.R., Opdenaker, L.M., Viswanathan, V., Fields, J.Z., and Boman, B.M. (2016). Somatostatin signaling via SSTR1 contributes to the quiescence of colon cancer stem cells. BMC Cancer *16*, 941.

Monteiro-Sepulveda, M., Touch, S., Mendes-Sá, C., André, S., Poitou, C., Allatif, O., Cotillard, A., Fohrer-Ting, H., Hubert, E.L., Remark, R., et al. (2015). Jejunal T Cell Inflammation in Human Obesity Correlates with Decreased Enterocyte Insulin Signaling. Cell Metab. *22*, 113–124.

Neis, E.P.J.G., Dejong, C.H.C., and Rensen, S.S. (2015). The role of microbial amino acid metabolism in host metabolism. Nutrients *7*, 2930–2946.

Oksanen, J., Blanchet, F.G., Kindt, R., Legendre, P., Minchin, P.R., O'hara, R.B., Simpson, G.L., Solymos, P., Stevens, M.H.H., and Wagner, H. (2013). Vegan: Community Ecology Package. R Package Version 2.0-2 (R Foundation for Statistical Computing).

Paddon-Jones, D., Westman, E., Mattes, R.D., Wolfe, R.R., Astrup, A., and Westerterp-Plantenga, M. (2008). Protein, weight management, and satiety. Am. J. Clin. Nutr. *87*, 1558S–1561S.

Patel, S. (2015). Emerging trends in nutraceutical applications of whey protein and its derivatives. J. Food Sci. Technol. *52*, 6847–6858.

Pfeuffer, M., and Jaudszus, A. (2016). Pentadecanoic and Heptadecanoic Acids: Multifaceted Odd-Chain Fatty Acids. Adv. Nutr. *7*, 730–734.

Pilvi, T.K., Korpela, R., Huttunen, M., Vapaatalo, H., and Mervaala, E.M. (2007). High-calcium diet with whey protein attenuates body-weight gain in high-fat-fed C57Bl/6J mice. Br. J. Nutr. *98*, 900–907.

Pimpin, L., Jebb, S.A., Johnson, L., Llewellyn, C., and Ambrosini, G.L. (2018). Sources and pattern of protein intake and risk of overweight or obesity in young UK twins. Br. J. Nutr. *120*, 820–829.

Poutahidis, T., Kleinewietfeld, M., Smillie, C., Levkovich, T., Perrotta, A., Bhela, S., Varian, B.J., Ibrahim, Y.M., Lakritz, J.R., Kearney, S.M., et al. (2013). Microbial reprogramming inhibits Western diet-associated obesity. PLoS ONE *8*, e68596.

Ran-Ressler, R.R., Khailova, L., Arganbright, K.M., Adkins-Rieck, C.K., Jouni, Z.E., Koren, O., Ley, R.E., Brenna, J.T., and Dvorak, B. (2011). Branched chain fatty acids reduce the incidence of necrotizing enterocolitis and alter gastrointestinal microbial ecology in a neonatal rat model. PLoS ONE *6*, e29032.

Rodrigues, R.R., Greer, R.L., Dong, X., DSouza, K.N., Gurung, M., Wu, J.Y., Morgun, A., and Shulzhenko, N. (2017). Antibiotic-Induced Alterations in Gut

Microbiota Are Associated with Changes in Glucose Metabolism in Healthy Mice. Front. Microbiol. *8*, 2306.

Rubio-Aliaga, I., Roos, Bd., Sailer, M., McLoughlin, G.A., Boekschoten, M.V., van Erk, M., Bachmair, E.M., van Schothorst, E.M., Keijer, J., Coort, S.L., et al. (2011). Alterations in hepatic one-carbon metabolism and related pathways following a high-fat dietary intervention. Physiol. Genomics *43*, 408–416.

Ruocco, C., Ragni, M., Rossi, F., Carullo, P., Ghini, V., Piscitelli, F., Cutignano, A., Manzo, E., Ioris, R.M., Bontems, F., et al. (2020). Manipulation of Dietary Amino Acids Prevents and Reverses Obesity in Mice Through Multiple Mechanisms That Modulate Energy Homeostasis. Diabetes *69*, 2324–2339.

Segata, N., Waldron, L., Ballarini, A., Narasimhan, V., Jousson, O., and Huttenhower, C. (2012). Metagenomic microbial community profiling using unique clade-specific marker genes. Nat. Methods *9*, 811–814.

Shi, S., Ji, X.-Y., Shi, J.-J., Shi, S.-Q., Jia, Q.-L., Yuan, G.-Z., Zhang, Q.-Y., Dong, Y., Lu, Y.-D., and Cui, H.-M. (2020). Gut Microbiota Mediates the Protective Effects of Andrographolide Inhibits Inflammation and Nonalcoholic Fatty Liver Disease (NAFLD) in High-Fat Diet induced ApoE (−/−) Mice. bioRxiv. https://doi.org/10.1101/2020.01.24.919316.

Shintani, T., Higashi, S., Suzuki, R., Takeuchi, Y., Ikaga, R., Yamazaki, T., Kobayashi, K., and Noda, M. (2017). PTPRJ Inhibits Leptin Signaling, and Induction of PTPRJ in the Hypothalamus Is a Cause of the Development of Leptin Resistance. Sci. Rep. *7*, 11627.

Simpson, S.J., and Raubenheimer, D. (2005). Obesity: the protein leverage hypothesis. Obes. Rev. *6*, 133–142.

Smart, K.F., Aggio, R.B., Van Houtte, J.R., and Villas-Bôas, S.G. (2010). Analytical platform for metabolome analysis of microbial cells using methyl chloroformate derivatization followed by gas chromatography-mass spectrometry. Nat. Protoc. *5*, 1709–1729.

Smith, H.A., Gonzalez, J.T., Thompson, D., and Betts, J.A. (2017). Dietary carbohydrates, components of energy balance, and associated health outcomes. Nutr. Rev. *75*, 783–797.

Solon-Biet, S.M., McMahon, A.C., Ballard, J.W., Ruohonen, K., Wu, L.E., Cogger, V.C., Warren, A., Huang, X., Pichaud, N., Melvin, R.G., et al. (2014). The ratio of macronutrients, not caloric intake, dictates cardiometabolic health, aging, and longevity in ad libitum-fed mice. Cell Metab. *19*, 418–430.

Spalinger, M.R., McCole, D.F., Rogler, G., and Scharl, M. (2015). Role of protein tyrosine phosphatases in regulating the immune system: implications for chronic intestinal inflammation. Inflamm. Bowel Dis. *21*, 645–655.

Stanstrup, J., Schou, S.S., Holmer-Jensen, J., Hermansen, K., and Dragsted, L.O. (2014). Whey protein delays gastric emptying and suppresses plasma fatty acids and their metabolites compared to casein, gluten, and fish protein. J. Proteome Res. *13*, 2396–2408.

Su, H., Mo, J., Ni, J., Ke, H., Bao, T., Xie, J., Xu, Y., Xie, L., and Chen, W. (2020). Andrographolide Exerts Antihyperglycemic Effect through Strengthening Intestinal Barrier Function and Increasing Microbial Composition of *Akkermansia muciniphila*. Oxid. Med. Cell. Longev. *2020*, 6538930.

Tahavorgar, A., Vafa, M., Shidfar, F., Gohari, M., and Heydari, I. (2014). Whey protein preloads are more beneficial than soy protein preloads in regulating appetite, calorie intake, anthropometry, and body composition of overweight and obese men. Nutr. Res. *34*, 856–861.

Thaiss, C.A., Itav, S., Rothschild, D., Meijer, M.T., Levy, M., Moresi, C., Dohnalová, L., Braverman, S., Rozin, S., Malitsky, S., et al. (2016). Persistent microbiome alterations modulate the rate of post-dieting weight regain. Nature *540*, 544–551.

van Dam, R.M., and Seidell, J.C. (2007). Carbohydrate intake and obesity. Eur. J. Clin. Nutr. *61* (*Suppl 1*), S75–S99.

Wickham, H. (2016). ggplot2: elegant graphics for data analysis (Springer).

Wolfe, R.R., Cifelli, A.M., Kostas, G., and Kim, I.Y. (2017). Optimizing Protein Intake in Adults: Interpretation and Application of the Recommended Dietary Allowance Compared with the Acceptable Macronutrient Distribution Range. Adv. Nutr. *8*, 266–275.

CellPress
OPEN ACCESS

STAR★METHODS

KEY RESOURCES TABLE

REAGENT or RESOURCE	SOURCE	IDENTIFIER
Chemicals, peptides, and recombinant proteins		
TRI Reagent	Sigma-Aldrich	Cat# 93289
Ampicillin	Domas-beta	Cat# 78917A
Neomycin	Sigma-Aldrich	Cat# N6386
Vancomycin	Macklin	Cat# V6062
Critical commercial assays		
RNeasy Mini Kit	QIAGEN	Cat# 74104
QIAamp PowerFecal DNA Kit	QIAGEN	Cat# 12830-50
Triglyceride Assay Kit	Abcam	Cat# ab65336
Mouse Glucose Assay Kit	CrystalChem	Cat# 81692
MILLIPLEX Metabolic Hormone Panel: leptin, resistin	Millipore	Cat# MMHMAG-44K; RRID:AB_2783855
MESO SCALE DIAGNOSTICS cytokine panel: IL-15, TNF-α, IP-10, CCL2	Meso Scale Discovery	Cat# K15069L-1
Growth hormone ELISA kit	Merck	Cat# EZRMGH-45K
IGF-1 ELISA kit	R&D systems	Cat# MG100; RRID:AB_2827989
Deposited data		
Data for Figure 1	Mendeley	doi: https://dx.doi.org/10.17632/3739n57bsn.1
Data for Figure 2	Mendeley	doi: https://dx.doi.org/10.17632/db5jzg8nsf.1
Data for Figure 3	Mendeley	doi: https://dx.doi.org/10.17632/486s9cr9d9.1
Data for Figure 7	Mendeley	doi: https://dx.doi.org/10.17632/7rb9x9xcw3.1
Data for Figure S1	Mendeley	doi: https://dx.doi.org/10.17632/8mpc9y9797.1
Data for Figure S2	Mendeley	doi: https://dx.doi.org/10.17632/wmp229s3xg.1
Data for Figure S3	Mendeley	doi: https://dx.doi.org/10.17632/537n7ppv9f.1
Data for Figure S6	Mendeley	doi: https://dx.doi.org/10.17632/7pznvxk5tt.1
Data for Figure S7	Mendeley	doi: https://dx.doi.org/10.17632/7rg8c34cpx.1
RNA-seq data	NCBI GEO	GEO: GSE167498
Microbiota shotgun metagenomics sequences: Study 1	EMBL-EBI ENA	ENA: PRJEB43357
Microbiota shotgun metagenomics sequences: Study 2	NMDC	NMDC: NMDC10017750
Experimental models: Organisms/strains		
Mouse: C57BL/6, Study 1	Envigo	Wildtype
Mouse: C57BL/6, Study 2	Charles River Laboratories	Wildtype
Software and algorithms		
SPSS	IBM	Version 24
IPA	Ingenuity Systems	https://www.qiagenbioinformatics.com
R platform	R Core Team	Version 3.6.1.
SAS 9.4	SAS Institute Inc	https://support.sas.com/en/support-home.html
R-studio	R Studio Team	Version 1.2.555
Inkscape	Inkscape	Version 0.92
GraphPad Prism version 7 for Windows	GraphPad software	https://www.graphpad.com/

RESOURCE AVAILABILITY

Lead contact

Further information for resources and reagents is displayed in Key resources table. Requests for resources should be directed to and will be fulfilled by the lead contact, Kanishka Nilaweera (Kanishka.nilaweera@teagasc.ie).

Materials availability

No novel reagents were generated by this study.

Data and code availability

RNA-seq data derived from mouse tissues are available at the Gene Expression Omnibus (GEO) data repository under the accession number (GSE167498).

DNA sequencing data of gut microbiota have been deposited to EMBL-EBI ENA and NMDS under the accession numbers PRJEB43357 (study 1) and NMDC10017750 (study 2) respectively.

Raw data from Figures 1, 2, 3, 7, S1–S3, S6, and S7 were deposited on Mendeley (see links in Key resources table).

EXPERIMENTAL MODEL AND SUBJECT DETAILS

Mice

Two studies were performed to assess the impact of dietary macronutrients on body composition (Study 1) and to explore the role of microbiota in mediating dietary effects on body weight gain (Study 2). All mice were male C57BL/6J WT and were commercially purchased from Envigo, UK and Charles River Laboratories, Beijing (study 1 and study 2, respectively).

Study 1

All animal procedures were licensed under the European Directive **2010/63/EU** and associated work adhered with University College Cork Animal Experimentation Ethics Committee (2015/ 007). Male C57BL/6J mice (Envigo, UK), aged 4-5 weeks, were purchased commercially (Envigo). All mice were group-housed (3 per cage) in individually ventilated cages with *ad libitum* access to food and water throughout the trial. Animals maintained in environmentally controlled conditions (45%–65% humidity, 20-22 ®C, 12:12 light-dark cycle (06:00-18:00)) and were monitored for health status on daily basis. Mice were fed a 20% kcal casein, 10% kcal fat and 70% kcal carbohydrate diet (Research Diets; USA; D12450Bi), until they were aged 20 weeks. Following 15 weeks of intake of the latter diet (at age 20 weeks), all animals were weight matched and randomly allocated to different groups and switched to experimental diets for 12 weeks, during which, the body weight and food intake was monitored on weekly basis. The dietary treatments consisted of 3 different levels of dietary fat (20, 40 and 55%) combined with 3 different levels of protein (10, 20 and 30%), each replicated with the protein coming from either casein (CAS) (diet codes: D17052701- D17052709) or whey protein isolate (WPI) (diet codes: D17052710- D17052718) (Table S1). The levels of cellulose and sucrose were fixed at 5% by weight and energy respectively. The 18 different treatments with 12 mice per group, where mice were housed in cages of 3 animals, with the exception of one dietary group (code) having 11 mice, making the total of 215 individual mice. The sample size was calculated based on our experience that protein quality (casein and WPI) has the smallest effect on total fat mass, individual fat depots (e.g., EAT) and other tissues (e.g., intestine) in diets varying in fat/carbohydrate quantity (McAllan et al., 2013). On average, to observe a 7.8% difference in total fat mass, which was the main driver of body weight, with 80% power at alpha = 0.05, a sample size of 12 was required. After 12 weeks of dietary interventions all animals were sacrificed and dissected into 24 different body components using protocol previously published (Mitchell et al., 2015). Animals were fasted for 12-16 hours prior to termination of the trial. At the end of the study, 5 animals were removed from the analysis due to the physical deformity.

Study 2

All animal procedures were approved by the animal ethical committee of the Institute of Genetics and Developmental Biology, Chinese Academy of Sciences (Beijing, China). Forty C57BL/6J male mice (Charles River Laboratories, Beijing) were caged in pairs between 22-24°C and subjected to a 12-hour light and dark cycle. They had previously been fed a standard low-fat baseline diet as our previous study (ID) from the age of 5 to 20 weeks. At the beginning of the experiment, when the mice were 20 weeks old, all individuals were weight matched and randomly allocated to one of 4 equally sized groups (10 in each) with 2 animals per cage. Two of the groups were allocated a 55% HFD containing casein (CAS) (diet code: D17052709) and the other two groups were given a 55% HFD containing whey protein isolate (WPI) (diet code: D17052718), where the protein quantity was at 30%. This initial period of the experiment lasted for 4 weeks (Figure 7A). After the initial period (4 weeks), 2 groups were given a course of antibiotics consisting of Ampicillin (1g/1L), Neomycin (1g/1L) and Vancomycin (0.5g/1L) (CAS-ABX, WPI-ABX). Previous study showed that these antibiotics had no impact on body weight (Rodrigues et al., 2017). The antibiotics were dissolved in the drinking water of the mice which was consumed *ad libitum.* The duration of antibiotic treatment was similar to the time course of other studies (Li et al., 2019; Thaiss et al., 2016). The treatment of the other two groups was unchanged throughout this period of the experiment (CAS-control, WPI-control). For the final 4 weeks of the experiment, the two control groups acted as faecal donors for the two groups which had received antibiotics (Figure 7A). The faecal samples used for the faecal transplants (FMT) were taken from all the cages of each of the control groups on the day of the transplant. The faeces were then added to water at a 1:6, faeces: water ratio and mixed until smooth under anaerobic conditions. This solution was then gavaged into one of the two antibiotic treated groups. WPI-FMT group received CAS fecal material and CAS-FMT group received WPI fecal material. Each mouse received 0.1 mL of the solution per gavage and the faecal transplants were carried out every 3 days until the end of the experiment. For the whole duration of the experiment, body weight and food intake

were measured twice a week. Faecal material was collected from all cages of mice before and after ABX treatment, half way through FMT period, and from individual animals at the end of FMT. This was stored at −80°C until required for sequencing.

METHOD DETAILS

RNA extraction, transcriptome analysis and qPCR

The hypothalamus, liver, and jejunum of all animals from 30% protein groups (6 diets [D17052703, D17052706, D17052709, D17052712, D17052715, D17052718], 71 animals) were collected. Total RNA was extracted from hypothalamic blocks using Tri-reagent (Sigma) and from liver and jejunum using the RNeasy Mini Kit (QIAGEN, 74104) according to manufacture instructions. Hypothalamic RNA was paired-end (PE) sequenced by PE100 on BGISEQ-500 platform at Beijing Genomic Institute (PE 2 × 75 bp, 150 bp per fragment, 20M read-pairs per sample). Sequencing of liver and jejunal RNA was performed using the NovaSeq 6000 platform (chemistry V4.0 Illumina) at Macrogen Inc Seoul, South Korea (PE 2 × 75 bp, 150 bp per fragment, 25M read-pairs per sample). Raw sequence reads were obtained in FASTQ format and these sequence reads were quality assessed using the software FastQC (v 0.111.58; https://www.bioinformatics.babraham.ac.uk/projects/fastqc/). Sequences from all samples were quality trimmed, and cleaned of adaptor sequences using BBDuk java package to trim Illumina adaptor sequences. On average 0.1% of the bases were trimmed per sample. Trimmed reads were aligned to the *Mus musculus* reference genome assembly GRCm38 (ftp://ftp.ensembl.org/pub/release-96/fasta/mus_musculus/dna/) using STAR RNA-seq aligner v2.5.2 (Dobin et al., 2013), and uniquely mapped read counts per Ensembl annotated gene/ transcript were estimated using the STAR–quantMode option. Genes with zero read counts across all samples as well as non-protein coding genes were removed prior to subsequent analysis. Differential gene expression analysis and data transformations and visualization were carried out using DeSeq2 v1.18.1 (Love et al., 2014) in R 3.5.2. Sample clustering was carried out on variance stabilizing transformed data and visualized using PCA. Differentially expressed genes lists were generated using a negative binomial generalized linear model and pairwise comparisons using each combination of fat and protein content in each tissue. P values were adjusted for multiple comparisons using a Benjamini and Hochberg (B-H) method. DE genes with an adjusted P value < 0.05 were used for further DE gene data exploration and pathway analysis.

The fold changes and p values were loaded into the Ingenuity Pathway Analysis (IPA) program (Ingenuity Systems; https://www.qiagenbioinformatics.com) for core analysis. IPA Knowledge Database was used to analyze the dietary impacts on canonical pathways and upstream regulators available in IPA. The overall results of IPA and differential gene expression analysis for three different tissues are presented in Table S3.

The EAT and SAT were collected from two dietary groups (D17052709 and D17052718) and RNA was extracted using the RNeasy Mini Kit. The mRNA level of target genes were measured in 600 ng of total RNA using Superscript II reverse transcriptase kit (Life Technologies) and subjected to Real-Time PCR as detailed elsewhere (McAllan et al., 2013; McManus et al., 2015). The corresponding gene expression was determined using $2^{-\Delta\Delta Cp}$ relative to the reference genes (beta-actin, Glyceraldehyde 3-phosphate dehydrogenase, Lactate dehydrogenase A and Hypoxanthine-guanine phosphoribosyltransferase). The primer sequences were as follows: *Fasn* (F: 5′-tccacctttaagttgccctg-3′; 5′-tctgctctcgtcatgtcacc-3′); *Glut4* (5′-ggcctgcccgaaagagtc-3′; 5′-aggagctggagcaaggac-3′).

Plasma metabolites and hormones

Blood was collected at the end of the trial. Plasma and fecal triglyceride levels were measured with the Triglyceride Quantification Assay kit (Abcam), plasma glucose was measured using the Mouse Glucose assay (Crystal Chem). Hormones were measured using ELISA kits (IGF1: R&D systems; growth hormone: Millipore), Milliplex kit (leptin and resistin: Millipore) and Meso Scale Discovery kit (TNF-α, IL-15, IP-10, CCL2/MCP-1) according to manufacturer's instructions.

Cecal and fecal microbiome

Microbial DNA extraction and sequencing. Genomic DNA was extracted and purified from cecal (Study 1) and fecal (Study 2) material using the QIAamp PowerFecal pro DNA kit (QIAGEN) according to the manufacturer's instructions. Total DNA was quantified with the Qubit dsDNA HS Assay kit (Thermo Fisher) in order to normalize DNA to 0.2 ng/μl for input to library preparation. Sequencing libraries for shotgun metagenomics sequencing were prepared from input DNA using the Nextera XT DNA Library Prep Kit (Illumina, 15031942). Library purification was achieved with AMPure magnetic beads (Beckman Coulter) at a ratio of 1:1.8 (DNA:AMPure). Libraries were sequenced on the NextSeq 500 platform operating on high-output run mode (kit chemistry V2.5, 300 Cycles) to generate 150-bp pair-end sequences in the Teagasc sequencing facility (Study 1) and in the Institute of Microbiology, Chinese Academy of Science, Beijing (Study 2), in accordance with standard Illumina sequencing protocols.

Bioinformatics processing and analysis. Quality control and removal of host contaminant reads from raw FASTQ sequencing files was performed with KneadData (V.0.72; https://github.com/biobakery/kneaddata) using Trimmomatic (V.0.38.1) (Bolger et al., 2014) and bmtagger (V.3.101) with *Mus musculus* (NCBI accession GCF_000001635) as host and standard options. Trimmed and joined FASTQ files were converted to FASTA using the *fq2fa* utility from IDBA (V.1.1.3) prior to supplying FASTA files to the Human Microbiome Project (HMP) Unified Metabolic Analysis Network (HUMAnN2, V.2.8.1) (Franzosa et al., 2018). HUMAnN2 was used with the UNIREF90 option and generated metabolic pathway models in addition to taxonomic profiles via the internal

call to Metagenomic Phylogenetic Analysis (MetaPhlAn2, V.2.9) (Segata et al., 2012) which were quantified as copies per million (cpm) and relative abundance (RA) respectively. Metabolic pathways were organized according to the MetaCyc hierarchy using the CatMap R package. Measures of alpha diversity and ordination of microbial data was achieved with the *vegan* R package (V.2.5-6) (Oksanen et al., 2013). Heatmaps were generated with the ComplexHeatmap R package (V.2.4.2) (Gu et al., 2016). All other graphical elements related to the microbiome were visualized with the R package ggplot2 (V.3.3.1) (Wickham, 2016), and in-house scripts. Version 3.6.1 of R was used to perform all such analyses. *Lactococcus lactis* was identified as contributing a significant number of reads to the microbial sequencing data, which was determined to result from the sterilized diets (data not shown). These values were excluded from analysis, and prior to the normalization of taxonomic and pathway profiles were removed.

Metabolomics of cecal content

Cecal water was prepared by homogenizing the cecal content (approx. 100 mg) with 400 μl of sterile water for 5 min using a bead beater. Samples were centrifuged at 16,000 g for 30 min, after which supernatants were filtered through 0.22 μm column filters (Costar). Two separate mass spectrometry methods were used to measure metabolites in each sample.

Method 1. Sample analysis was carried out by MS-Omics (Denmark) as follows. Prior to analysis, 20 μl extracts were mixed with 180 μl 10mM ammonium formate with 0.1% formic acid. The analysis was carried out using a Thermo Scientific Vanquish LC coupled to Thermo Q Exactive HF MS. An electrospray ionization interface was used as ionization source. Analysis was performed in negative and positive ionization mode. The UPLC was performed using a slightly modified version of the protocol described by Catalin et al. (UPLC/MS Monitoring of Water-Soluble Vitamin Bs in Cell Culture Media in Minutes, Water Application note 2011, 720004042en). Peak areas were extracted using Compound Discoverer 2.0 (Thermo Scientific). Identification of compounds were performed at four levels; Level 1: identification by retention times (compared against in-house authentic standards), accurate mass (with an accepted deviation of 3ppm), and MS/MS spectra, Level 2a: identification by retention times (compared against in-house authentic standards), accurate mass (with an accepted deviation of 3ppm). Level 2b: identification by accurate mass (with an accepted deviation of 3ppm), and MS/MS spectra, Level 3: identification by accurate mass alone (with an accepted deviation of 3ppm). Selected metabolites are shown in Figure S6B.

Method 2. Sample analysis was carried out by MS-Omics as follows. Samples were derivatized with methyl chloroformate using a slightly modified version of the protocol described by Smart et al. (2010). All samples were analyzed in a randomized order. Analysis was performed using gas chromatography (7890B, Agilent) coupled with a quadrupole mass spectrometry detector (5977B, Agilent). The system was controlled by ChemStation (Agilent). Raw data was converted to netCDF format using Chemstation (Agilent), before the data was imported and processed in MATLAB R2018b (Mathworks, Inc.) using the PARADISe software described by Johnsen et al. (2017). Selected metabolites are shown in Figures S6C and S6D.

Liver fatty acid analysis

Fatty acid extraction from liver tissue was performed using the previously published protocol (Rubio-Aliaga et al., 2011). Liver fatty acids were analyzed by GC-MS. The frozen sample was resuspended in 300μL of hexane and vortexed vigorously for 1 min. Then 100μL of sample was combined with another 300μL of hexane to dilute the sample, and 200μL solution was transferred to GC vial with 250μL insert. The fatty acid composition of liver tissue was analyzed using GC-qTOF-MS (Agilent Technologies) consisting of a 7890B GC system, and a 7200 qTOF mass spectrometer. The column used was an Agilent HP-5MS 5% Phenyl Methyl Siloxane (Dimension: 30 m × 250 μm × 0.25 μm). Helium was used as the carrier gas with a flow rate of 1.2 mL/min and the temperature of the injector was 250°C. The sample was run under splitless mode and the injection volume was 1 μL. Separation was performed under the following temperature: 70°C for 2 mins, 15°C /min to 190°C and 190°C for 1 min, 5°C/min to 230°C and 230°C for 5 mins, 20°C/min up to 300°C and 300°C for 5 mins. The total run time is 32.5 mins. The Agilent 7200 qTOF-MS was operated in the electron ionization (EI) mode at 70 eV, a MS source temperature of 230°C, MS quad temperature of 150°C, and in the scan range of m/z 50–650. The identification of fatty acid was based on fatty acid methyl ester (FAME) standards.

QUANTIFICATION AND STATISTICAL ANALYSIS

Statistical analyses were performed using SPSS 24(IBM), SAS 9.4, and the R statistical programming environment (V.3.6.1) Values are presented as mean ± SEM or boxplots with minimum, maximum and median. Univariate factorial ANOVA was used to analyze the effect of dietary factors on body weight, energy intake, body composition, plasma hormones, cytokines and metabolites. General Liner model (GLM)/repeated-measures (RM) ANOVA was used to compare data across treatment period. Where appropriate, following factorial ANOVA or GLM/RM, post hoc Bonferroni test was used, to isolate the differences between individual diets. Significance was accepted at $p < 0.05$. Linear regression analysis performed using SAS 9.4. Normality tests were performed on all data using Kolmogorov-Smirnov test and if necessary, log normalization or other transformation procedure was used prior to analysis. The independent samples t test followed by false discovery rate procedure was used to analyze the statistical differences between the groups for cecal and liver metabolites. Non-parametric tests were used to analyze measures related to microbiome data, with all such analysis performed in R. Pairwise comparisons were done with the Wilcoxon Rank-Sum test from the *stats* package and PERMANOVA using the adonis2 function in the *vegan* package. NMDS dissimilarity matrices were assessed with the analysis of

similarities (ANOSIM) test, while PCoA matrices were assessed with adonis2, both as implemented in the vegan package. Tests were corrected for multiple comparisons using the qvalue package (V.2.20.0; https://github.com/StoreyLab/qvalue) and a false discovery rate (FDR) adjusted p value of pFDR < 0.05 to define significance. Murine body composition analysis was carried out in R (V.3.6.1) and R-studio (V.1.2.555). Principal component analysis (for body composition analysis; Figure 2A) was performed in base R, biplot was constructed and plotted using the ggplot2 library and the adonis PERMANOVA implementation from the vegan library was used for statistical testing, using euclidean distance as a distance metric.

Cell Reports, Volume *35*

Supplemental information

Protein quality and quantity influence the effect of dietary fat on weight gain and tissue partitioning via host-microbiota changes

Oleksandr Nychyk, Wiley Barton, Agata M. Rudolf, Serena Boscaini, Aaron Walsh, Thomaz F.S. Bastiaanssen, Linda Giblin, Paul Cormican, Liang Chen, Yolanda Piotrowicz, Davina Derous, Áine Fanning, Xiaofei Yin, Jim Grant, Silvia Melgar, Lorraine Brennan, Sharon E. Mitchell, John F. Cryan, Jun Wang, Paul D. Cotter, John R. Speakman, and Kanishka N. Nilaweera

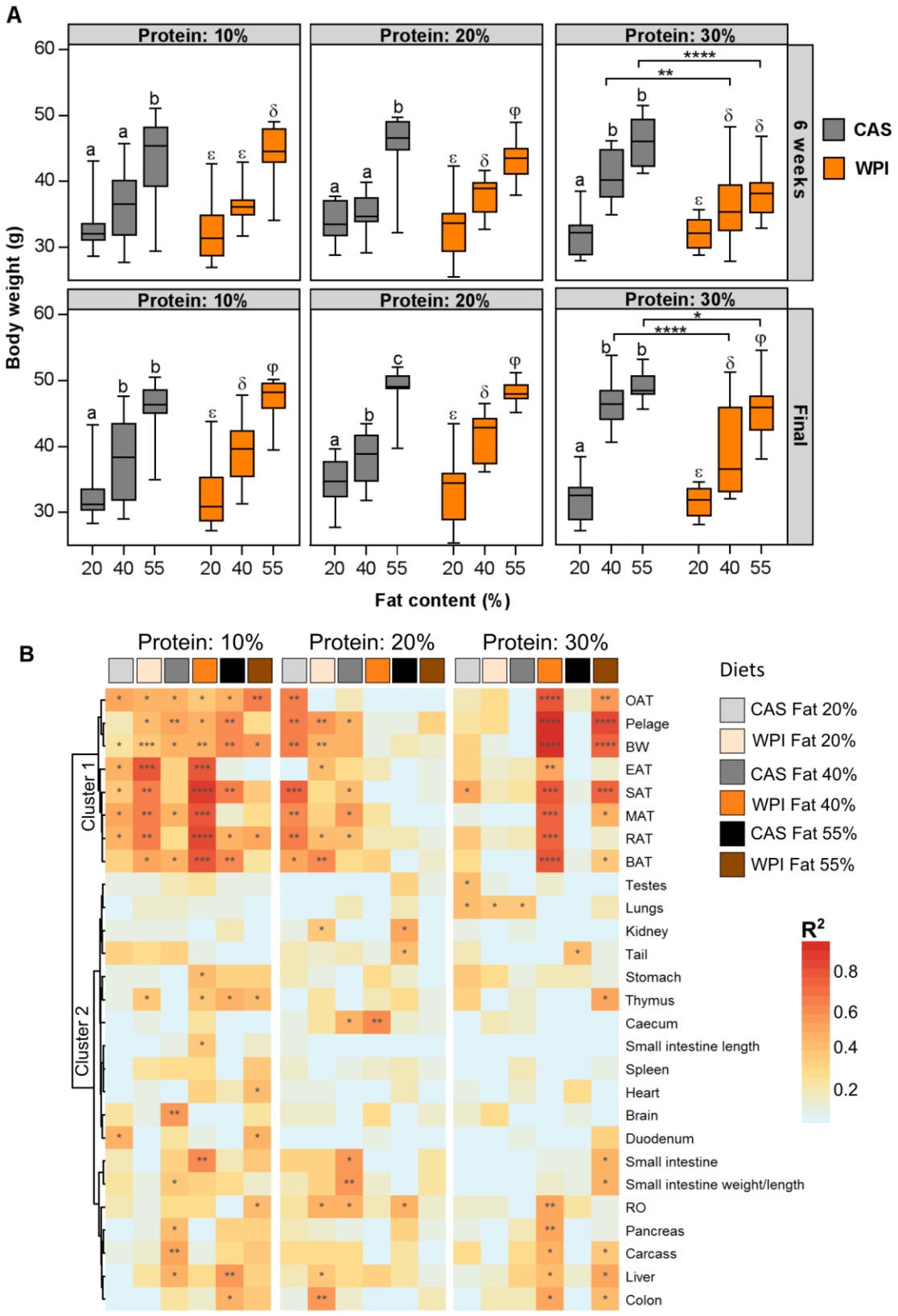

Figure S1. BW changes after 6 and 12 weeks of dietary interventions and correlation of IGF-1 with body weight and tissue weight, **Related to Figure 1 and 2.** (A) BW at 6 (upper panel) and 12 weeks (lower panel). Groups were compared within different fat contents (CAS, English and WPI Greek letters) and protein type (CAS vs WPI). Values are represented as boxplots. Group with the same letters

were not significantly different ($p > 0.05$). (B) Correlation coefficients (R^2) and p-values of IGF-1 vs BW and tissue weight. The scale for the correlations: increasing intensity of orange/red indicates positive correlation. Dendrogram shows the similarity in responses of the different organs to BW changes. P-value range (*$p < 0.05$, **$p < 0.01$; ***$p < 0.001$; ****$p < 0.0001$). N = 11-12 biologically independent samples. See Table S2 for the results of pairwise comparison of BW according to protein content.

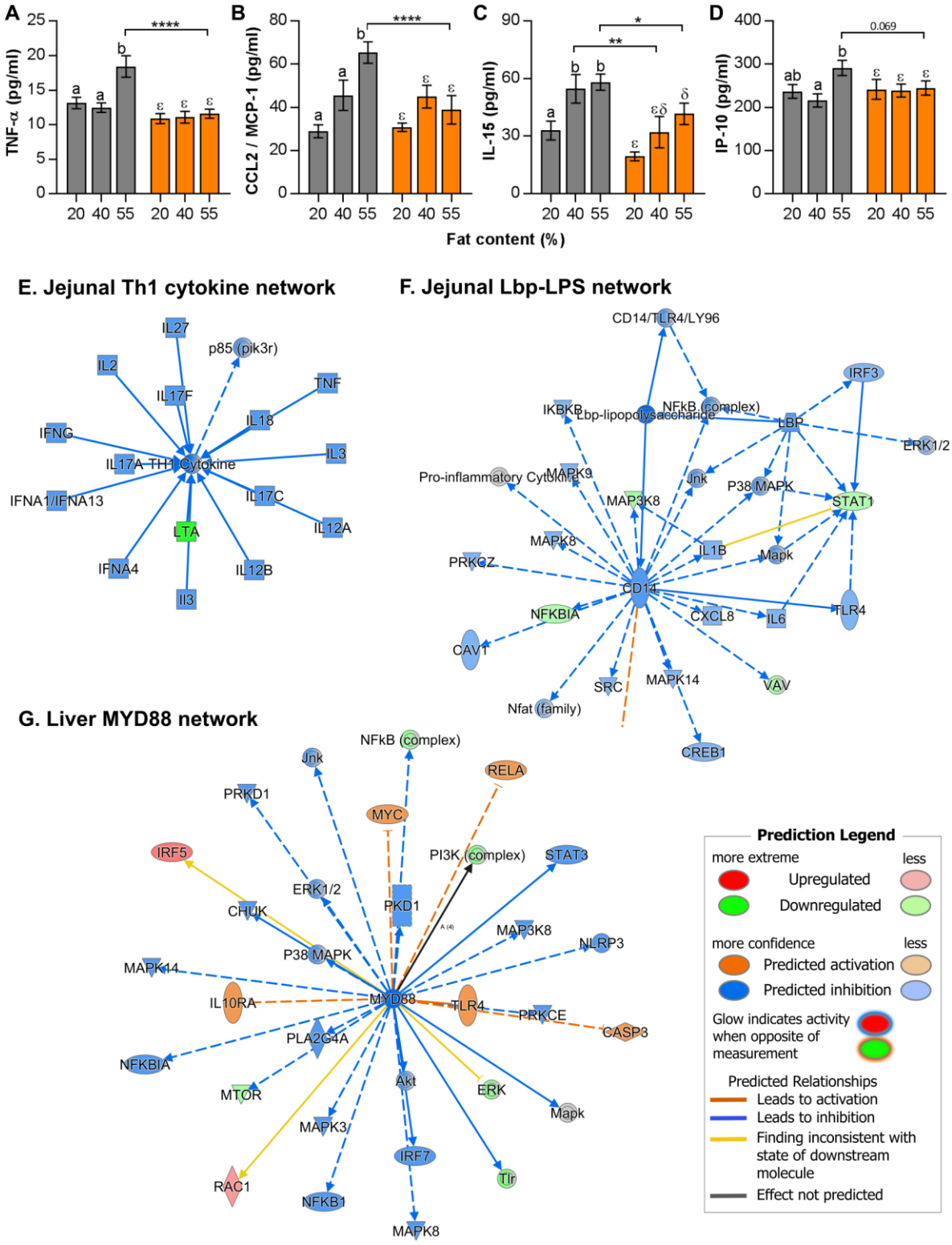

Figure S2. Plasma profile of cytokines and causal networks associated with the transcriptome in the jejunum and the liver responding to 30% protein with variable fat and protein type (% energy), Related to Figure 3, 4 and 5. (A-D) TNF-α, CCL2/MCP-1, IL-15 and IP-10 plasma levels. Groups were compared within different fat contents (CAS, English and WPI Greek letters) and protein type (CAS vs WPI). N = 6-10 biologically independent samples and 2 technical replicates. P-value range (*p < 0.05, **p < 0.01; ***p < 0.001; ****p < 0.0001). (E-G) Networks predict (E, F) inhibition of Th1

cytokine (z-score = - 8.7) and lbp (LPS-binding protein) – LPS (z-score = - 6.5) in the jejunum of WPI relative to CAS, and (G) inhibition of MYD88 causal network (z-score = - 4.2) in the liver of WPI relative to CAS ($p < 0.05$ for E-G). Causal networks are based on IPA analysis of the transcriptome data with subsequent predicted effects on downstream regulators. Figure parenthesis shows the relationship between molecules within the network. N = 11-12 biologically independent samples. TNF-α: Tumour necrosis factor α; CCL2/MCP-1: C-C motif chemokine ligand 2/monocyte chemoattractant protein; IL-15: Interleukin 15; IP-10: Interferon gamma-induced protein 10.

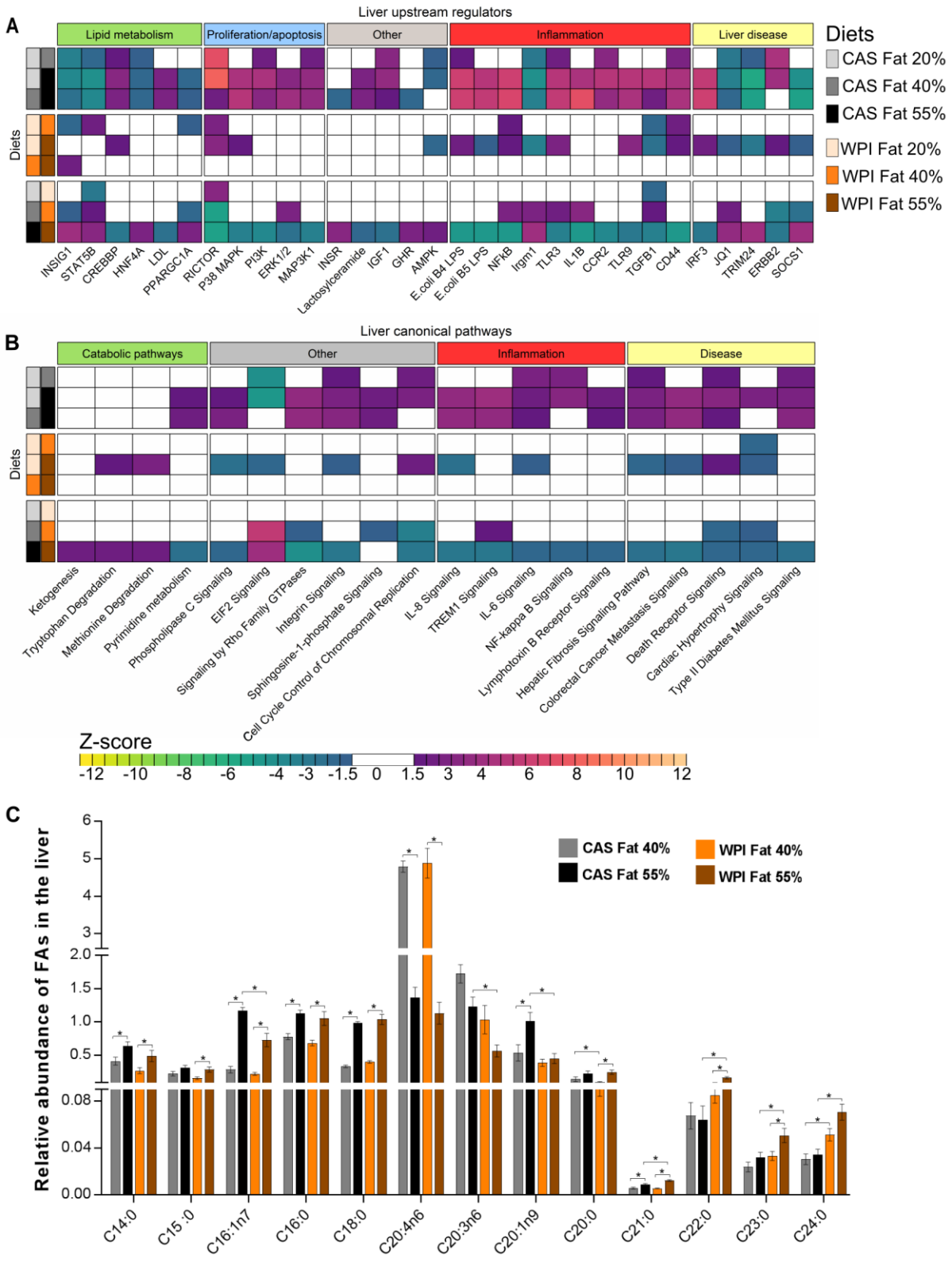

Figure S3. Liver transcriptome associated pathways and fatty acid profiles affected by 30% proteins with variable fat and protein type (% energy), Related to Figure 5. (A, B) Heatmaps showing significant changes ($p < 0.05$) in selected upstream regulators (A) and canonical pathways (B) with activation z-scores > 1.5 (activation) or < -1.5 (inhibition), white coloured cells indicate insignificant changes in selected pathways/regulators. Data derived from IPA analysis of the transcriptome data.

See Table S4 for IPA statistics and pathway/regulator target molecules. (C) Fatty acid profile of the liver detected by GC-MS. Values are represented as mean ± SEM. P-values: *p < 0.05. N = 11-12 biologically independent samples.

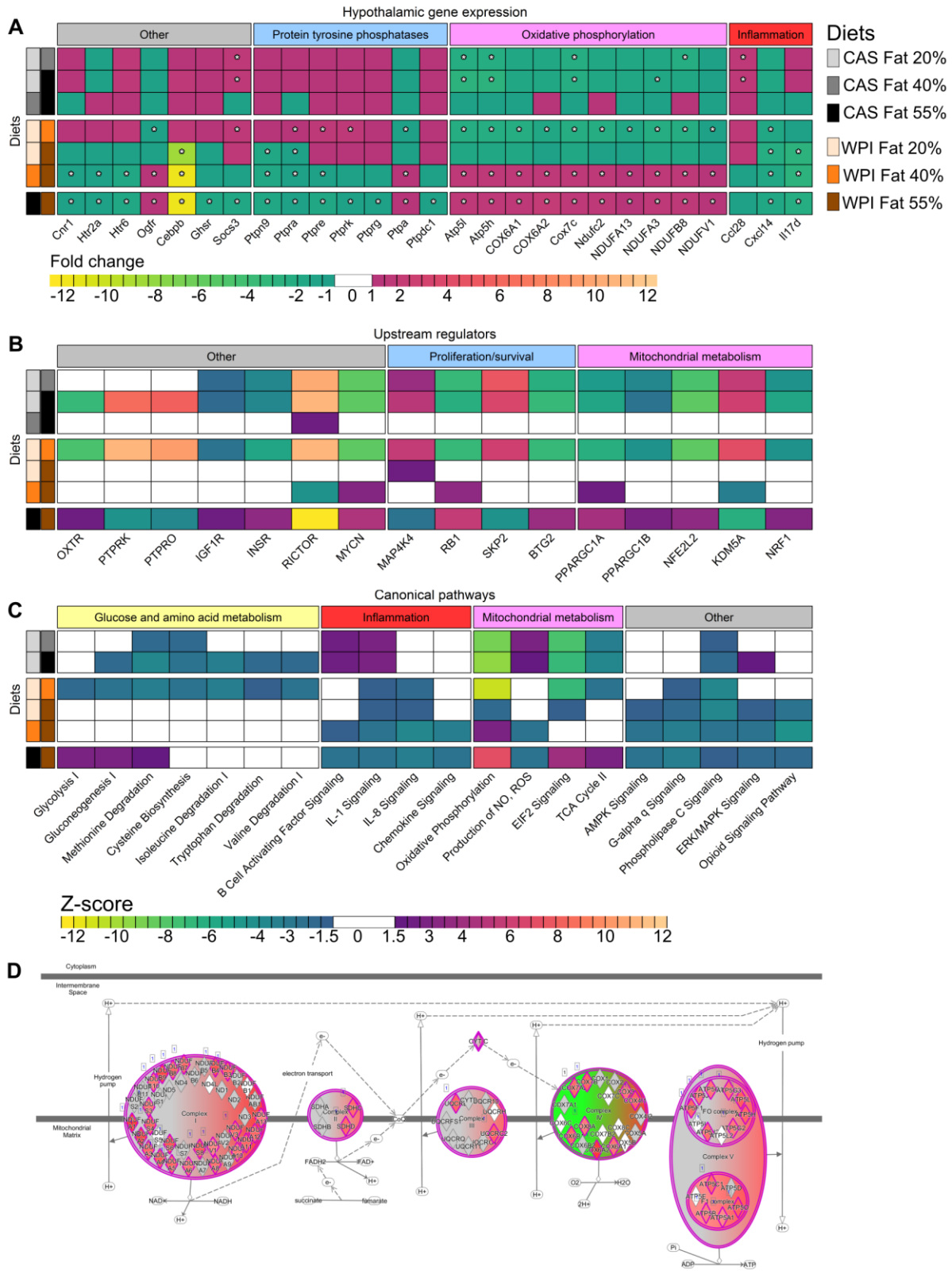

Figure S4. Hypothalamic expression of genes and activation of upstream regulators and canonical pathways affected by 30% proteins with variable fat and protein type (% energy), Related to Figure 4 and 5. (A-C) Heatmaps shows significant changes in gene expression, upstream regulators (B) and canonical pathways (C). The values are represented as log2 fold changes (A) and

z-scores (B, C) between corresponding diets. * p-value < 0.05 (A); activation z-scores > 1.5 (activation) or < -1.5 (inhibition) with p < 0.05 (B, C), white coloured cells indicate insignificant changes in selected pathways/regulators. (D) Oxidative phosphorylation pathway (z-score 6.94, p < 0.05) of WPI relative to CAS at 55% fat, see legend from Figure S3. The heatmaps were generated by IPA analysis of the transcriptome data (B, C). N = 11-12 biologically independent samples. See Table S4 for IPA statistics and pathway/regulator target molecules.

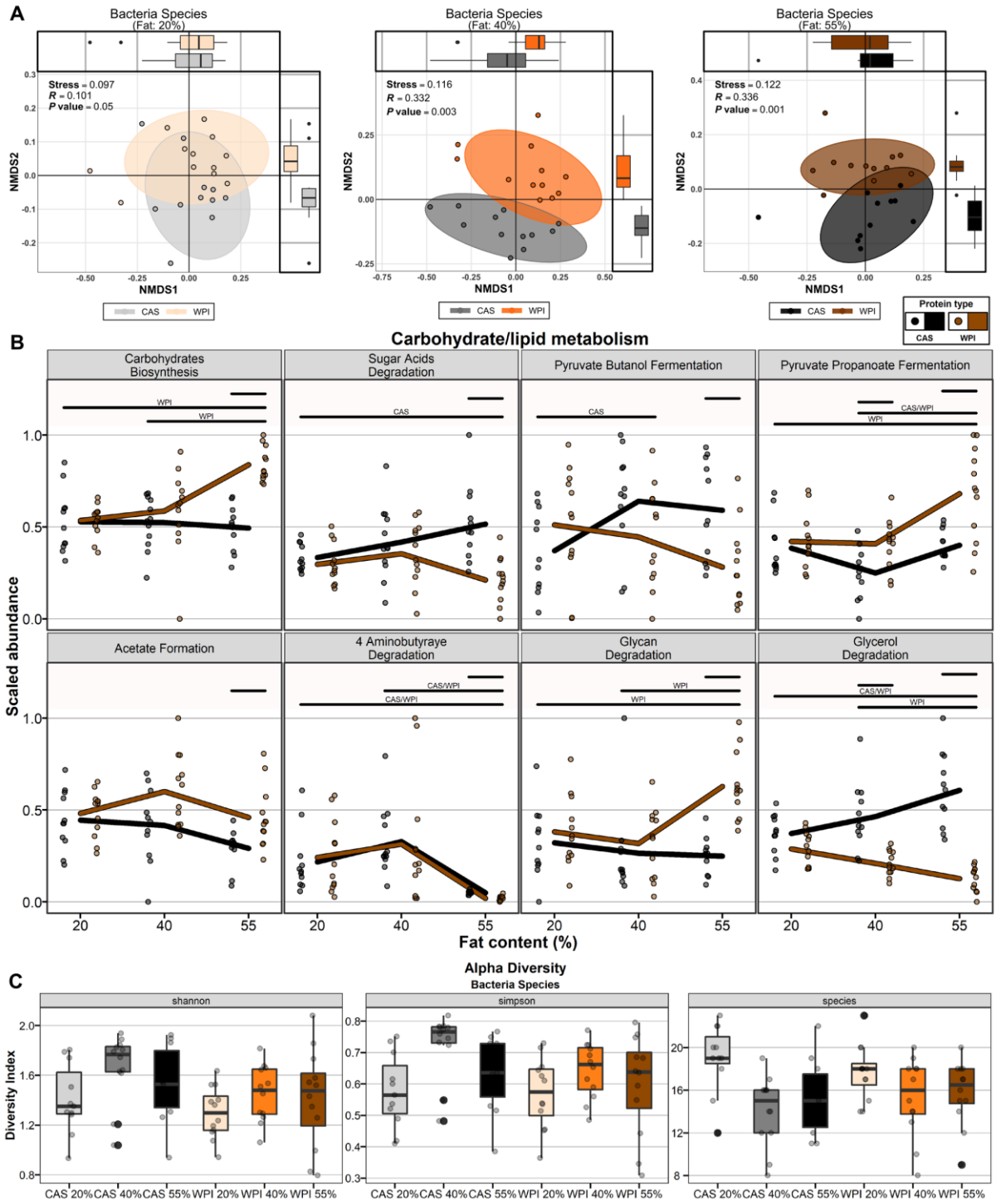

Figure S5. Effects of 30% protein diets on the cecal microbiome, Related to Figure 6. (A) Ordination of Bacteria species at 20, 40 and 55% fat for both protein types. (B) Selected carbohydrate and lipid metabolism pathways. Solid bars indicate significance (adjusted Wilcoxon rank sum $p < 0.05$). Within protein group comparisons are indicated by WPI or CAS, while cross-group differences for fat percentage are designated with blank bars. (C) Alpha-diversity of Bacteria species for both protein groups at 20, 40 and 55% fat. N = 11-12 biologically independent samples.

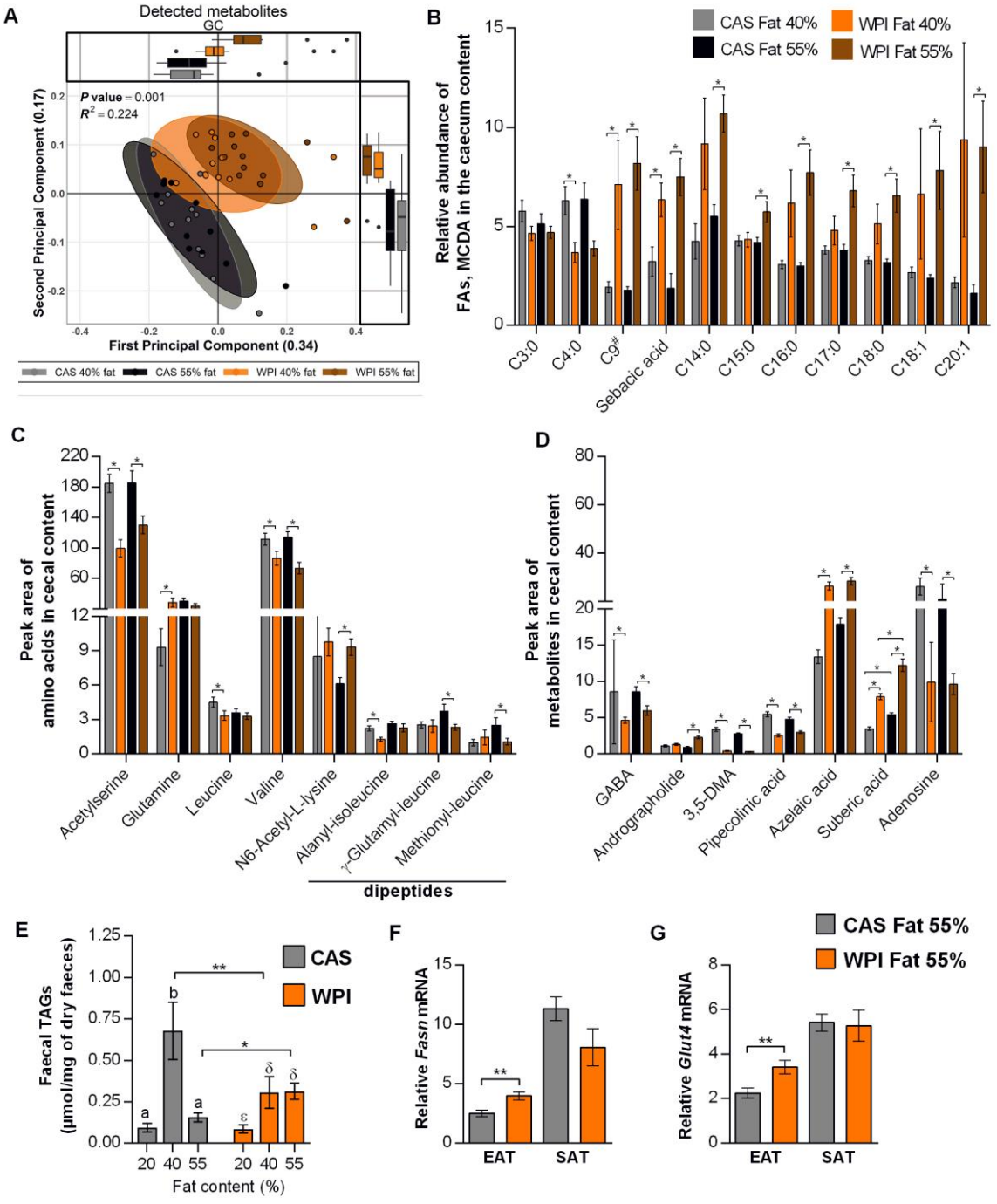

Figure S6. Effect of 30% protein diet and metabolic profile of caecum content and expression of *Fasn* and *Glut4* mRNA in EAT and SAT, Related to Figure 6. (A) PCA of cecal metabolites detected by GC-MS. (B) FA profile of caecum content detected by GC-MS. (C, D) Amino acids, dipeptides (C) and selected metabolites (D) of cecal content detected by LC-MS. (E) Fecal TAG content. BCFA: C9# (2,4-Dimethylpimelic acid). MCDA: medium chain dicarboxylic acid. (F, G) mRNA expression of *Fasn* (F) and *Glut4* (G) in EAT and SAT. Values are represented as mean ± SEM. P-values: *p < 0.05, **p < 0.01, ***p < 0.001, ****p < 0.0001. N = 10-12 biologically independent samples (A-G), N = 2 technical replicates (E-G).

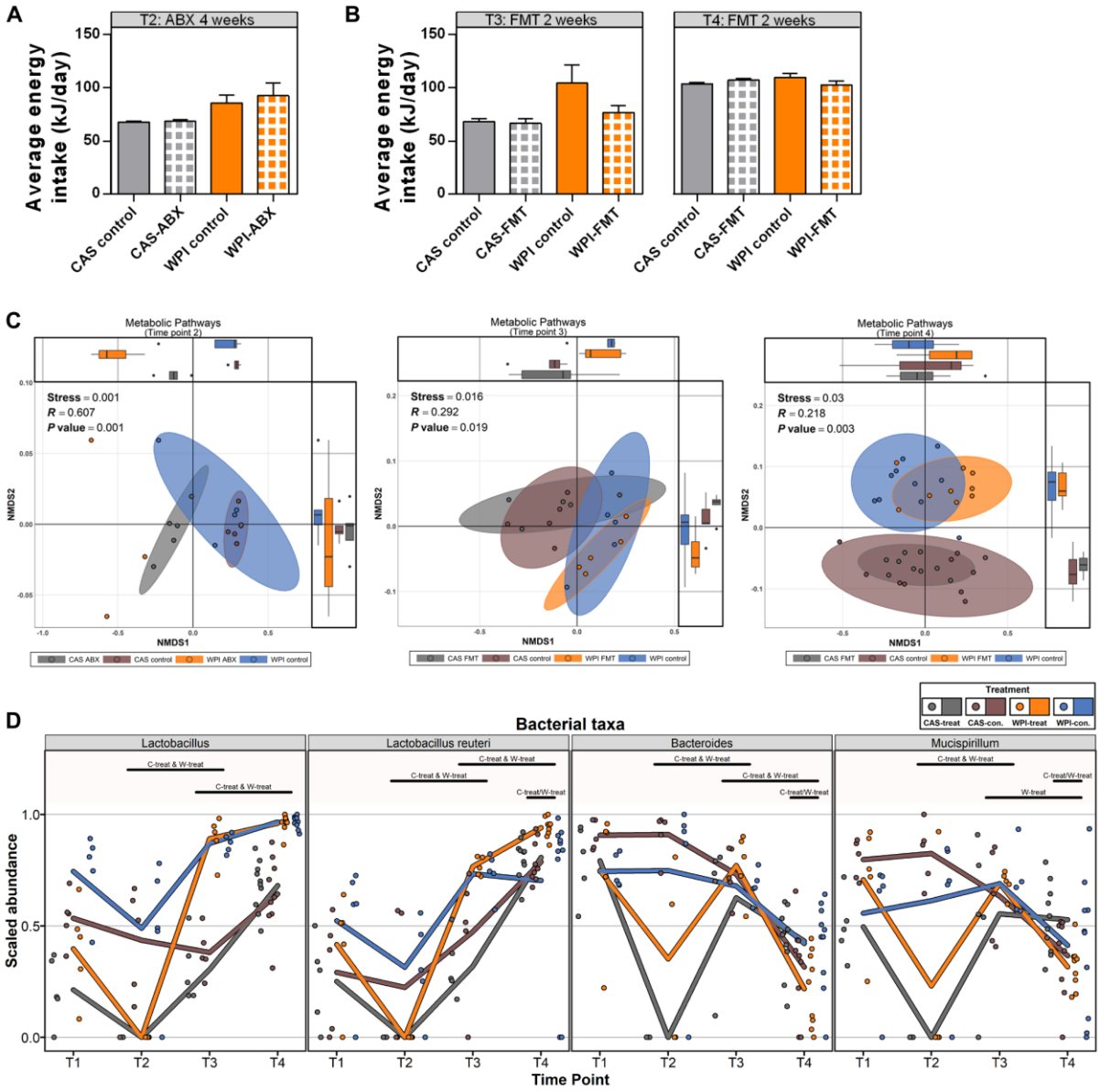

Figure S7. The impact of antibiotic treatment and FMT on energy intake and gut microbiome, Related to Figure 7. (A, B) Energy intake changes during ABX (A) and FMT (B) experiment. (C) Beta-diversity of pathways demonstrated by PCoA ordination. (D) Selected bacterial taxa. Solid bars indicate significance (adjusted Wilcoxon rank sum $p < 0.05$). Group comparisons are indicated by the following abbreviations: C-treat (CAS treatment) and W-treat (WPI treatment). C-treat/W-treat: comparison between treatment groups; C-treat & W-treat: comparison across time points. For bioinformatic analysis, the fecal samples were collected per cage at T1-T3 and from individual animals at T4. N = 9-10 biologically independent samples.